



European Reviews of Chemical Research

Has been issued since 2014.
E-ISSN 2413-7243
2019. 6(1). Issued 2 times a year

EDITORIAL BOARD

Bekhterev Viktor – Sochi State University, Sochi, Russian Federation (Editor in Chief)
Belskaya Nataliya – Ural Federal University, Ekaterinburg, Russian Federation
Kuvshinov Gennadiy – Sochi State University, Sochi, Russian Federation
Elyukhin Vyacheslav – Center of Investigations and Advanced Education, Mexico, Mexico
Kestutis Baltakys – Kaunas University of Technology, Kaunas, Lithuania
Mamardashvili Nugzar – G.A. Krestov Institute of Solution Chemistry of the Russian Academy of Sciences, Ivanovo, Russian Federation
Maskaeva Larisa – Ural Federal University, Ekaterinburg, Russian Federation
Md Azree Othuman Mydin – Universiti Sains Malaysia, Penang, Malaysia
Navrotskii Aleksandr – Volgograd State Technical University, Volgograd, Russian Federation
Ojovan Michael – Imperial College London, London, UK

Journal is indexed by: **CrossRef** (UK), **Electronic scientific library** (Russia), **Journal Index** (USA), **Open Academic Journals Index** (USA), **ResearchBib** (Japan), **Scientific Indexing Services** (USA)

All manuscripts are peer reviewed by experts in the respective field. Authors of the manuscripts bear responsibility for their content, credibility and reliability.

Editorial board doesn't expect the manuscripts' authors to always agree with its opinion

Postal Address: 1367/4, Stara Vajnorska str., Bratislava – Nove Mesto, Slovakia, 831 04
Release date 15.06.19.
Format 21 × 29,7/4.

Website: <http://ejournal14.com/en/index.html> Headset Georgia.
E-mail: aphr.sro@gmail.com

Founder and Editor: Academic Publishing House Researcher s.r.o. Order № 114.

European Reviews of Chemical Research

2019

Is. **1**

CONTENTS

Articles and Statements

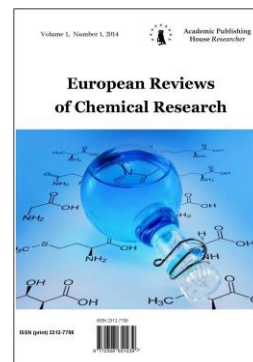
Theoretical Study of the Regioselectivity of the Reaction Between Diethyl(Trichloromethyl)Phosphonate and Triethylphosphite Using the DFT Method A. Barhoumi, M. El idrissi, A. Zeroual, S. Bakkas, A. El Hajbi, A. Tounsi	3
Quantum Mechanical Descriptors of Indazole-Containing Derivatives Using the DFT Method H. Essassaoui, M. El idrissi, R. Bouhdadi, M. Echajia, A. Zeroual, A. Tounsi, M. Mbarki	12
Experimental and Theoretical Elaboration of Phase Diagram for the Ternary System Ni(NO ₃) ₂ -Al(NO ₃) ₃ -H ₂ O at 20°C M. Jouaiti, B. Mekkaoui, A. Barroug, M. El idrissi, R. Lbibb, L. Lâallam, A. Jouaiti	23
Synthesis of Different Classes of Polyheterocyclic Cyanine Dyes: a Review H.A. Shindy	29

Copyright © 2019 by Academic Publishing House Researcher s.r.o.



Published in the Slovak Republic
European Reviews of Chemical Research
Has been issued since 2014.
E-ISSN: 2413-7243
2019, 6(1): 3-11

DOI: 10.13187/erch.2019.1.3
www.ejournal14.com



Articles and Statements

Theoretical Study of the Regioselectivity of the Reaction Between Diethyl(Trichloromethyl)Phosphonate and Triethylphosphite Using the DFT Method

A. Barhoumi ^a, M.El idrissi ^{b,*}, A. Zeroual ^a, S. Bakkas ^a, A. El Hajbi ^a, A. Tounsi ^b

^a Chouaïb Doukkali University, El Jadida, Morocco

^b Moulay Slimane University, Beni Mellal, Morocco

Abstract

In this study we used the DFT/B3LYP/6-311G(d,p) quantum mechanical method to propose a theoretical explanation of the regioselectivity observed experimentally in the reaction between diethyl(trichloromethyl)phosphonate and triethylphosphite using a variety of approaches, notably frontier molecular orbital theory and calculation of activity energies and reactivity indices. Our results show that triethylphosphite functions as a nucleophile while diethyl(trichloromethyl)phosphonate behaves as an electrophile. The nucleophilic attack takes place preferentially at the chlorine atom of diethyl (trichloromethyl)phosphonate rather than at the carbon, and the reaction is polar and regioselective.

Keywords: triethylphosphite, diethyl(trichloromethyl)phosphonate, DFT/B3LYP/6-311G(d,p), reactivity indices, activation energy.

1. Introduction

Organophosphorus compounds are increasingly used in modern organic chemistry because of their potential in such varied domains as biology (Akbaş et al., 2013; Mudryk et al., 2015), medicine (Cupistiet al., 2013; Dabrzalska et al., 2015), agriculture (as plant growth regulators) and biochemistry (Engel et al., 2003). They are also of great interest as precursors in organic synthesis (Kann et al., 2003; Bricklebank et al., 2003). This versatility arises from the variable valency of phosphorus (Ellis et al., 2006; Gilheany et al., 1992).

Bibliographic research shows that the reaction of the trivalent phosphorus derivatives $[(RO)_3P, (RO)_2PR', \dots]$ with certain polyhalogenoalkanes ($CCl_4, BrCCl_3, \dots$) leads to the formation of a number of products (Waschbüsch et al., 1996; Nai et al., 1997) some of which have numerous applications in industry and biology (Halazy et al., 1996). The reactivity of trivalent phosphorus with regard to polyhalogenomethanes has already been the subject of several studies (Barhoumi et al., 2018; Bakkas et al., 2000). This reactivity varies according to the nature of the substituents carried by the phosphorus atom and increases as its electropositivity increases.

Our aim in this work was to carry out a theoretical study, using DFT/B3LYP/6-311G(d, p), of the reactivity of $CCl_3PO(OEt)_2$ with triethylphosphite in order to determine whether the

* Corresponding author

E-mail addresses: idrissi_82@hotmail.fr (M. El idrissi)

phosphorus attacks the carbon or the chlorine of the diethyl(trichloromethyl)phosphonate (Figure 1).

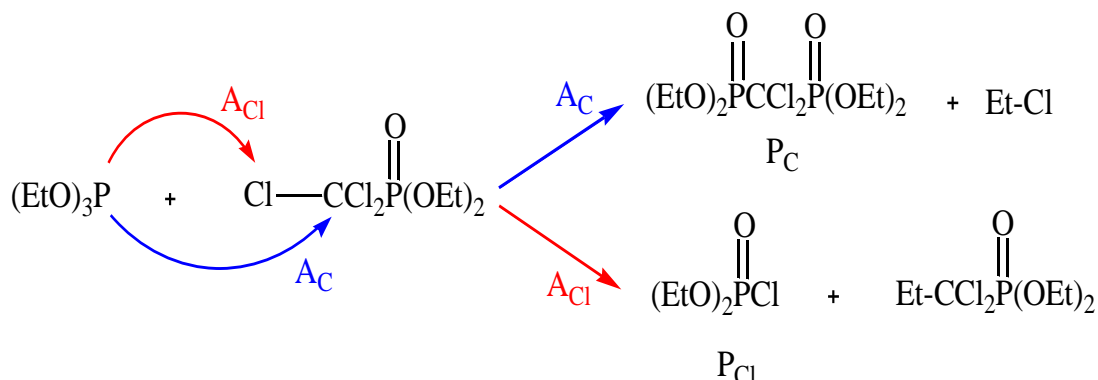


Fig. 1. Reaction between diethyl(trichloromethyl)phosphonate $\text{CCl}_3\text{PO}(\text{OEt})_2$ and triethylphosphite $(\text{EtO})_3\text{P}$

2. Method of calculation

The mechanism and the equilibrium geometries of the reaction between diethyl(trichloromethyl)phosphonate and triethylphosphite, as well as the transition states corresponding to the two approaches at A_C and A_{Cl} , were studied using density functional theory DFT (Parr et al., 1989; Deng et al., 1995) with base B3LYP/6-311G (d, p) (Becke et al., 1993; Lee et al., 1988). Transition states were localized and their existence confirmed by the presence of a single imaginary frequency in the Hessian matrix. The Intrinsic Reaction Coordinate (IRC) was calculated (Fukui et al., 1981a; Fukui et al., 1981b) and plotted in order to show that the transition state is indeed linked to the two minima (reactants and products). Values of enthalpy, entropy and free energy were calculated using standard statistical thermodynamics (Hehre et al., 1986). The reactivity indices were calculated from the HOMO and LUMO energies in the base state of the molecules using DFT/B3LYP/6-311G (d,p). All calculations were carried out with Gaussian 09 software (Frischet al., 2009).

3. Results and discussion

3.1. Structural optimisation of the reactants

Table 1 shows atomic distances and bond energies of the reactant atoms of diethyl(trichloromethyl)phosphonate in its most stable form, showing that all the chlorine atoms don't have the same reactivity with regard to the most nucleophilic site of triethylphosphite. These parameters were optimised using Gaussian 09 software. Energy analysis shows that the fundamental state of triethylphosphite stabilises at -804.8978 a.u and that of diethyl(trichloromethyl)phosphonate at -2144.4342 u.a , in other words that triethylphosphite is more reactive.

Table 1. Bond energy and interatomic distance of the reactant atoms in diethyl (trichloromethyl)phosphonate

$X - Y$	$d(X - Y)$	$E(X - Y) \text{ Kcal/mol}$
$C_1 - Cl_2$	1.795	474.899
$C_1 - Cl_3$	1.803	471.937
$C_1 - Cl_{22}$	1.793	476.467

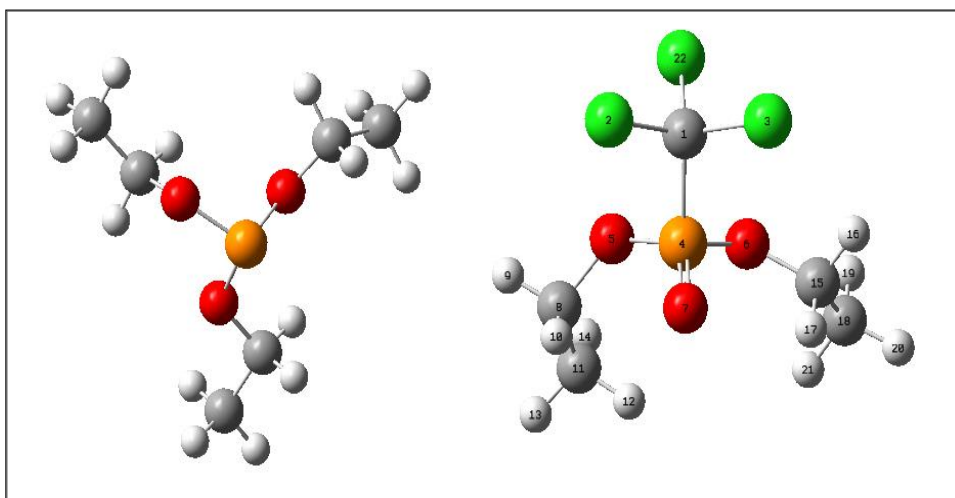


Fig. 2. The most stable structure of the two reactants $(\text{EtO})_3\text{P}$ and $\text{CCl}_3\text{PO}(\text{OEt})_2$.

3.2. Study of the frontier orbitals

We calculated the HOMO/LUMO energy gap for the two possible combinations of the two reactants

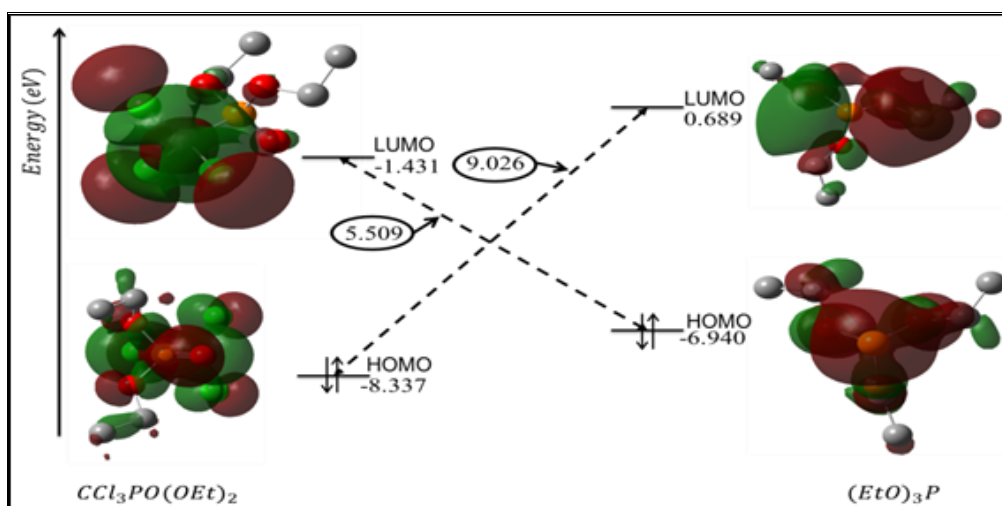


Fig.3. Energy gap (eV) between the HOMO of triethylphosphite $(\text{EtO})_3\text{P}$ and the LUMO of diethyl(trichloromethyl)phosphonate $\text{CCl}_3\text{PO}(\text{OEt})_2$.

Frontier molecular orbital theory (FMO) makes it possible to analyse the reactivity of molecules in terms of the interactions between the molecular orbitals of the reactants by taking account of only the most important interactions (Rauk et al., 1994). The orbitals considered in studying the interaction between two reactants are the HOMO (highest occupied molecular orbital) of the one and the LUMO (lowest unoccupied molecular orbital) of the other, chosen in such a way that the $E_{\text{LUMO}} - E_{\text{HOMO}}$ energy gap is as small as possible (Mebi et al., 2011). As a general rule, the smaller the difference between the orbitals of the two reactants, the stronger the interaction between these orbitals, and the greater the stabilising effect. As Figure 4 shows, the orbital diagramme gives a good idea of the reactivity of the system. We can see that the main interaction takes place between the LUMO of diethyl(trichloromethyl)phosphonate and the HOMO of triethylphosphite.

Localisation of the molecular orbitals of triethylphosphite and diethyl(trichloromethyl)phosphonate shows that the HOMO is very concentrated around the phosphorus atom, while the LUMO is concentrated around the chlorine atom (Figure 4). This indicates that the nucleophilic attack by the phosphorus atom takes place essentially at the chlorine atom.

3.3. Chemical concepts and reactivity indices derived using DFT

In order to determine which reactant behaves as a nucleophile (electron donor) and which as an electrophile (electron acceptor), we calculated the HOMO/LUMO energy gaps between them (Table 2).

Table 2. Difference between the two possible HOMO/LUMO combinations for diethyl(trichloromethyl)phosphonate $\text{CCl}_3\text{PO}(\text{OEt})_2$ and triethylphosphite $(\text{EtO})_3\text{P}$ (eV).

Reactants	E_{LUMO}	E_{HOMO}	$ E_{\text{HOMO}((\text{EtO})_3\text{P})} - E_{\text{LUMO}} $	$ E_{\text{HOMO}} - E_{\text{LUMO}(\text{CCl}_3\text{PO}(\text{OEt})_2)} $
$(\text{EtO})_3\text{P}$	0.689	-6.940	5.509	9.026
$\text{CCl}_3\text{PO}(\text{OEt})_2$	-1.431	-8.337		

Our results show that the $|E_{\text{HOMO}((\text{EtO})_3\text{P})} - E_{\text{LUMO}}|$ gap is smaller than the $|E_{\text{HOMO}} - E_{\text{LUMO}(\text{CCl}_3\text{PO}(\text{OEt})_2)}|$ gap, showing that triethylphosphite behaves as a nucleophile while diethyl(trichloromethyl)phosphonate behaves as an electrophile.

The global indices defined using conceptual DFT/B₃LYP (Geerlings et al., 2003) are valuable tools for studying the reactivity of polar interactions. The static global properties electronic chemical potential μ , chemical hardness η , global electrophilicity index ω and global nucleophilicity index N are chemical properties which enable us to analyse reactivity.

We calculated the electronic chemical potential μ and global hardness η from the energies of the HOMO and LUMO frontier molecular orbitals, as $\mu = \frac{E_{\text{HOMO}} + E_{\text{LUMO}}}{2}$ and $\eta = E_{\text{LUMO}} - E_{\text{HOMO}}$ respectively (Parr et al., 1989). The global electrophilicity index ($\omega = \mu^2/2\eta$) (Parr et al., 1983) is defined as the energy stabilisation due to charge transfer. It has been shown that the nucleophile character of a molecule can be calculated without taking account of its electron density. The nucleophilicity index N is expressed in terms of the HOMO energy of tetracyanoethylene (TCE) as $N = E_{\text{HOMO}(\text{NU})} - E_{\text{HOMO}(\text{TCE})}$ (Pérez et al., 2009). These values, together with maximum charge transfer ΔN_{max} (Domingo et al., 1994) and the global electrophilicity gap $\Delta\omega$ are shown in Table 3.

Table 3. HOMO and LUMO energy, electronic chemical potential μ , hardness η , electrophilicity ω , global nucleophilicity N , maximum charge transfer ΔN_{max} and global electrophilicity gap $\Delta\omega$ between $(\text{EtO})_3\text{P}$ and $\text{CCl}_3\text{PO}(\text{OEt})_2$ (eV)

Reactants	E_{LUMO}	E_{HOMO}	μ	η	ω	N	$\Delta\omega$	ΔN_{max}
$(\text{EtO})_3\text{P}$	0.689	-6.940	-3.125	7.629	0.640	2.428	...	0.409
$\text{CCl}_3\text{PO}(\text{OEt})_2$	-1.431	-8.337	-4.884	6.906	1.727	1.031	1.087	0.707

$$\begin{cases} E_{\text{HOMO}(\text{TCE})} = -9.368 \text{ eV} \\ \Delta N_{\text{max}} = -\mu/\eta \end{cases}$$

Our results show that diethyl(trichloromethyl)phosphonate $\text{CCl}_3\text{PO}(\text{OEt})_2$ behaves as an electrophile while triethylphosphite $(\text{EtO})_3\text{P}$ behaves as a nucleophile. Diethyl(trichloromethyl)phosphonate has the highest electrophilicity index ($\omega = 1.727 \text{ eV}$) and the lowest nucleophilicity index ($N = 1.031 \text{ eV}$). Additionally, the electronic chemical potential of $(\text{EtO})_3\text{P}$ ($\mu = -3.125 \text{ eV}$) is situated at a higher energy level than that of ($\mu = -4.884 \text{ eV}$), $(\text{EtO})_3\text{P} > \mu(\text{CCl}_3\text{PO}(\text{OEt})_2)$, in other words a stream of electrons circulating

from $(\text{EtO})_3\text{P}$ to $\text{CCl}_3\text{PO}(\text{OEt})_2$ stabilises the system. These results confirm that triethylphosphite behaves as a nucleophile and diethyl(trichloromethyl)phosphonate as an electrophile in this reaction.

The maximum charge transfer of ($\Delta N_{\text{max}} = 0.707 \text{ eV}$) is greater than that of triethyl phosphite ($\Delta N_{\text{max}} = 0.409 \text{ eV}$) and the electrophilicity gap ($\Delta\omega = 1.087 \text{ eV}$) between diethyl(trichloromethyl)phosphonate and triethylphosphite is high, showing that the reaction is polar.

3.4. Kinetic and thermodynamic study of the nucleophilic modes of attack of $(\text{EtO})_3\text{P}$ on $\text{CCl}_3\text{PO}(\text{OEt})_2$ (A_{Cl} and A_{C})

3.4.1. Thermodynamic study

We studied the feasibility and the regioselectivity of the reaction between diethyl(trichloromethyl)phosphonate $\text{CCl}_3\text{PO}(\text{OEt})_2$ and triethylphosphite $(\text{EtO})_3\text{P}$ from a thermodynamic point of view. In order to compare the reactivity of the two modes of attack (A_{C} and A_{Cl}), we calculated the differences in reaction energy ΔE_{r} , reaction enthalpy ΔH_{r} and free enthalpy ΔG_{r} corresponding to the formation of compounds P_{C} and P_{Cl} (Table 4).

Table 4. Calculated values (Kcal/mole) of the differences in reaction energy ΔE_{r} , reaction enthalpy ΔH_{r} and free enthalpy ΔG_{r} .

Reactants	Product	ΔH_{r}	ΔE_{r}	ΔG_{r}
$(\text{EtO})_3\text{P} + \text{CCl}_3\text{PO}(\text{OEt})_2$	P_{C}	-24.606	-25.400	-21.283
	P_{Cl}	-44.501	-45.637	-42.630

As Table 4 shows, variations in free enthalpy ΔG_{r} are negative whatever the mode of attack. It follows that these reactions are possible and are thermodynamically favoured. We also found that the variation in free enthalpy ΔG_{r} corresponding to the formation of compound P_{Cl} is greater in absolute terms than that corresponding to the formation of compound P_{C} . The formation of compound P_{C} resulting from an attack on the carbon atom A_{C} is thermodynamically less favoured than the formation of compound P_{Cl} . Free enthalpy of formation of the latter is greater in absolute terms than that of compound P_{C} . The value of ΔE_{r} corresponding to the formation of compound P_{Cl} is greater in absolute terms than that corresponding to the formation of compound P_{C} . This shows that the most favourable site for an attack is the halogen Cl rather than the carbon C .

3.4.2. Structure and energy of the transition states

In order to determine the more favoured mode of attack (A_{C} or A_{Cl}), and thus the most favoured product of the reaction between triethylphosphite and diethyl(trichloromethyl)phosphonate, we localised the transition states and calculated the activation barriers for the two possible reaction pathways. The transition states TS_{C} and TS_{Cl} , corresponding to the two modes of attack, were localised. These two transition states were confirmed by the presence of one and only one negative eigenvalue in the force constant matrix: in other words there is a single imaginary frequency in the Hessian matrix, corresponding to the vibration mode of the formation of the bonds $\text{P} - \text{CCl}_2$ and $\text{P} - \text{Cl}$ respectively and the splitting of bonds $\text{C} - \text{Cl}$ and $\text{C} - \text{CCl}_2$ respectively. The two transition states TS_{C} and TS_{Cl} are shown in Figure 5.

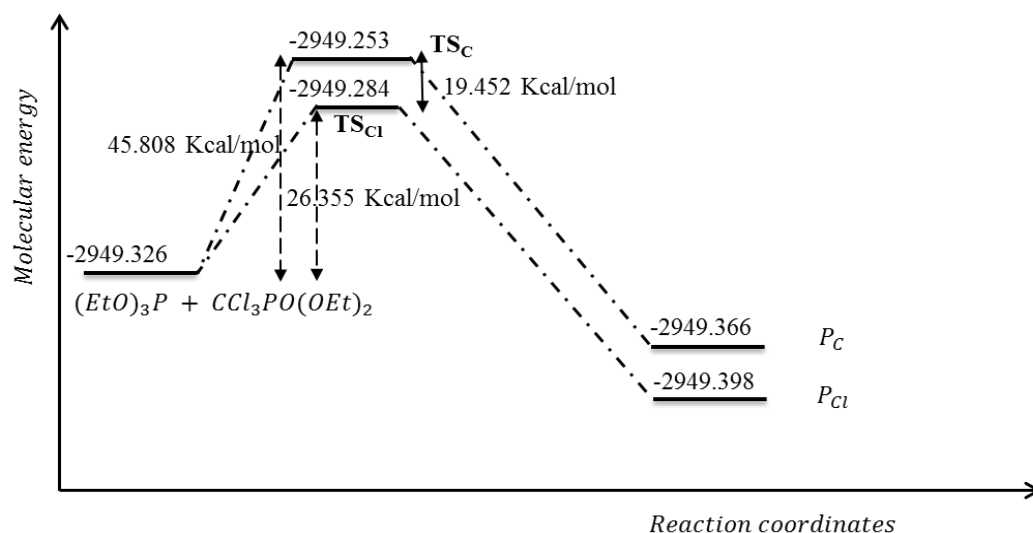


Fig. 5. Energy profile in (u. a) of the reaction between diethyl (trichloromethyl) phosphonate and triethylphosphite

The potential energy surface (PES) corresponding to the two modes of attack shows that the energy of the transition state corresponding to the attack on the chlorine atom TS_{Cl} is 19.452 Kcal/mol below the energy of the transition state corresponding to the attack on the carbon atom TS_C . The activation energy is 45.808 Kcal/mol for A_C and 26.355 Kcal/mol for A_{Cl} . In other words, the attack on the chlorine atom is kinetically preferred to the attack on the carbon atom.

We can conclude from this theoretical investigation that, while both modes of attack by triethylphosphite on trichloromethylphosphine oxide (A_{Cl} and A_C) are thermodynamically possible, the products formed by the attack on the chlorine atom are kinetically and thermodynamically preferred.

The structure of the transition state associated with reaction pathway A_{Cl} is more stable than that associated with A_C . The two structures optimised using DFT/B3LYP/6-311G(d,p) are shown in Figure 6. Phosphite tends to react more with chlorine than with carbon because of the difference in length between bonds $P - CCl_2$ and $P - Cl$ in the transition state ($P - Cl < d(P - Cl_2)$).

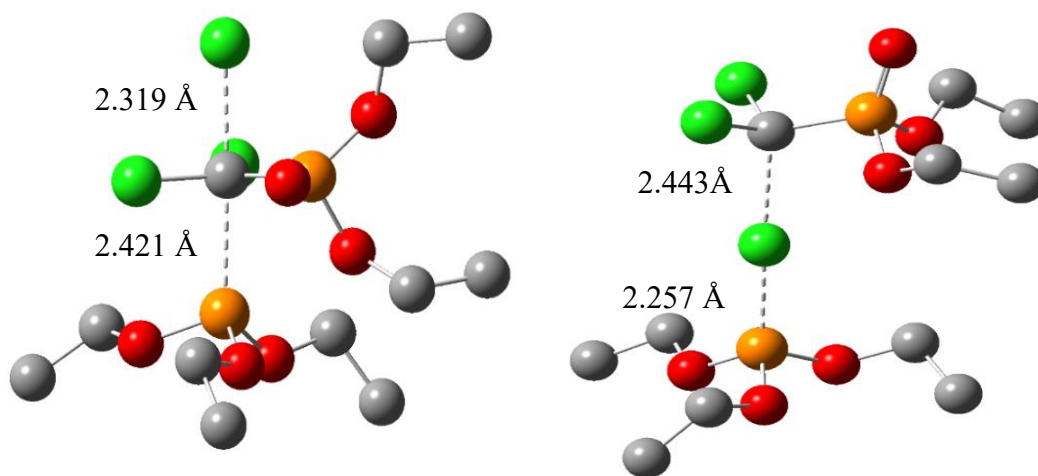


Fig. 6. Bond lengths of the transition states in the reaction between triethylphosphite and diethyl(trichloromethyl)phosphonate

3.5. Determination of the intrinsic reaction coordinates (IRC).

On the basis of the optimised geometry of the transition state we calculated the IRC (Intrinsic Reaction Coordinate) (Lee et al., 1988; Fukui et al., 1981) in order to confirm that the transition state indeed links the reactants and the products. Figure 7 presents the reaction pathway corresponding to the two modes of attack and shows that the transition state is indeed linked to the two minima (reactants and products).

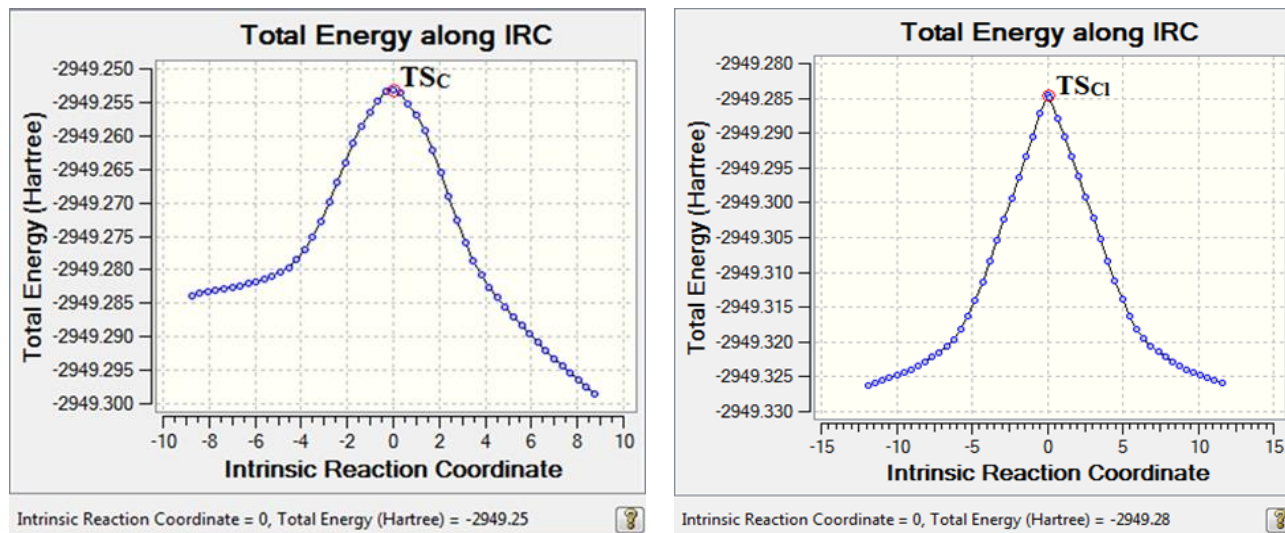


Fig. 7. IRC of the reaction between triethylphosphite and diethyl(trichloromethyl)phosphonate (A_{Cl}/A_C)

Natural population analysis of the reaction shows that the charge transfer from the nucleophile to the electrophile is 0.554(e) for transition state TS_C and 0.648(e) for transition state TS_{Cl} . This indicates that TS_{Cl} is more stable and favorable, and that the reaction is polar in character. These results confirm the findings obtained from the HOMO/LUMO energy gaps and the global indices ω , N and μ .

4. Conclusion

Theoretical study of the reaction between diethyl(trichloromethyl)phosphonate $CCl_3PO(OEt)_2$ and triethylphosphite $(EtO)_3P$ using DFT/B3LYP/6-311G (d, p) shows that whatever the mode of attack of the phosphorus atom (A_{Cl} and A_C) on diethyl(trichloromethyl)phosphonate, the corresponding variations in free enthalpy ΔG_r are negative, indicating that these attacks are thermodynamically possible. Calculation of the global indices shows that triethyl phosphite behaves as a nucleophile and diethyl(trichloromethyl)phosphonate as an electrophile. The reaction is characterised by a relatively high charge transfer, implying a polar mechanism. The variation in reaction enthalpy ΔH_r is highly exothermic for the reaction leading to formation of compound P_{Cl} . Consequently this reaction is favoured, since the products formed are stable and their formation releases energy. Localisation of the HOMO of triethylphosphite and the LUMO of diethyl(trichloromethyl)phosphonate shows that the phosphorus atom is the nucleophile centre of the former while the chlorine atom is the electrophile centre of the latter. The thermodynamic and kinetic study shows that the stable products of the reaction between diethyl(trichloromethyl)phosphonate and triethylphosphite are those resulting from the attack on the chlorine atom.

5. Conflict of interest

The authors declare that there is no conflict of interests regarding the publication of this paper. Also, they declare that this paper or part of it has not been published elsewhere.

References

- Akbaş et al., 2013 – Akbaş H., Okumuş A., Kılıç Z., Hökelek T., Süzen Y., Koç L.Y., Açık L., Çelik Z.B. (2013). Synthesis, and spectroscopic, thermal and dielectric properties of phosphazene based ionic liquids: OFET application and tribological behavior. *Eur. J. Med. Chem.*, 70: 294-307.
- Bakkas et al., 2000 – Bakkas S., Mouzdahir A., Khamliche L., Julliard M., Péralez E., Chanon M. (2000). Facile Synthesis of Fluorinated Phosphonates via Photochemical and Thermal Reactions. *Phosphorus, Sulfur and Silicon*, 157: 211-224.
- Barhoumi et al., 2018 – Barhoumi A., Bakkas S., El Hajbi A. (2018). Theoretical study of the chemical reactivity of the reaction between Trichloromethyl phosphine oxide and triethyl phosphite using the DFT method. *Mor. J. Chem*, 6: 414-424.
- Becke et al., 1993 – Becke A.D. (1993). A new mixing of Hartree-Fock and local density-functional theories. *J. Chem. Phys.*, 98: 1372-1377.
- Bricklebank et al., 2003 – Bricklebank N. (2003). Organophosphorus ester-induced chronic neurotoxicity. *Organophosphorus Chem.*, 33, 289-320.
- Cupisti et al., 2013 – Cupisti Zadeh A., Kalantar-Zadeh K. (2013). Management of natural and added dietary phosphorus burden in kidney disease. *Seminars in Nephrology*, 33: 180-190.
- Dabrzalska et al., 2015 – Dabrzalska M., Zablocka M., Mignani S., Majoral J.P., Maculewicz B.K. (2015). Complexing Methylene Blue with Phosphorus Dendrimers to Increase Photodynamic Activity. *Int. J. Pharm.*, 492: 266-274.
- Deng et al., 1995 – Deng L., Ziegler T. (1995). Anisotropic Metal Nanoparticles: Synthesis, Assembly, and Optical Applications. *Phys. Chem.*, 99: 612-618.
- Domingo et al., 1994 – Domingo L.R., Chamorro E., Pérez P. (1994). Understanding the Reactivity of Captodative Ethylenes in Polar Cycloaddition Reactions. A Theoretical Study. *J. Org. Chem.*, 73, 4615-4624.
- Ellis et al., 2006 – Ellis B., Macdonald C.L.B. (2006). Inorg. Phosphorus(I) Iodide: A Versatile Metathesis Reagent for the Synthesis of Low Oxidation State Phosphorus Compounds. *Chem.*, 45: 6864-6874.
- Engel et al., 2003 – Engel R., Cohen J.L.I. (2003). Synthesis of Carbon-Phosphorus Bonds, 2nd ed., CRC Press, Boca Raton.
- Frisch et al., 2009 – Frisch M.J. (2009). Gaussian 09, Revision D.01, Gaussian, Inc., Wallingford CT.
- Fukui et al., 1981a – Fukui K. (1981). Formulation of the reaction coordinate. *J. Phys. Chem.*, 74: 4161-4163.
- Fukui et al., 1981b – Fukui K. (1981). The path of chemical reactions - the IRC approach. *Acc. Chem. Res.*, 14: 363-368.
- Geerlings et al., 2003 – Geerlings P., De proft F., Langenaeker W. (2003). Conceptual Density Functional Theory. *Chem. Rev.*, 103: 1793-1873.
- Gilheany et al., 1992 – D.G. Gilheany in Hartley F. R. (ed.). The Chemistry of Organophosphorus Compounds, Wiley, Chichester, England, 2: 1-52.
- Halazy et al., 1996 – Halazy S., Ehrhard A., Eggenspieler A., Berges-Gross V., Danzin C. (1996). Synthesis of fluorophosphonylated acyclic nucleotide analogues via copper(I)-catalyzed Huisgen 1-3 dipolar cycloaddition. *Tetrahedron*, 52: 177-184.
- Hehre et al., 1986 – Hehre W.J., Schleyer L.R., Pople J.A. (1986). Ab initio Molecular Orbital Theory, Wiley, New York.
- Kann et al., 2003 – Kann N., Rein, T. (2003). Synthesis and cytotoxic activity of a new potential DNA bisintercalator: 1,4-Bis{3-[N-(4-chlorobenzo[g]phthalazin-1-yl)aminopropyl]}piperazine. *Synthesis*, 13: 579-595.
- Lee et al., 1988 – Lee C., Yang W., Parr R.G. (1988). Development of the Colle-Salvetti correlation-energy formula into a functional of the electron density. *Phys. Rev.*, B 37, 785-789.
- Mebi et al., 2011 – Mebi C.A. (2011). DFT study on structure, electronic properties, and reactivity of cis-isomers of [(NC₅H₄-S)₂Fe(CO)₂]. *J. Chem. Sci.*, 123: 727-731.
- Mudryk et al., 2015 – Mudryk Z., Perliński P., Antonowicz J., Robak D., Mar. (2015). Number of bacteria decomposing organic phosphorus compounds and phosphatase activity in the sand of two marine beaches differing in the level of anthropopressure. *Pollut. Bull*, 101: 566-574.

[Nai et al., 1997](#) – Nai H.K., Burton D.J. (1997). Using Ferroelectric Poling to Change Adsorption on Oxide Surfaces. *J. Am. Chem. Soc.*, 119: 9137-9143.

[Parr et al., 1983](#) – Parr R.G., Pearson R.G. (1983). Absolute hardness: companion parameter to absolute electronegativity. *J. Am. Chem. Soc.*, 105: 7512-7516.

[Parr et al., 1989](#) – Parr R.G., Yang W. (1989). Density Functional Theory of Atoms and Molecules, Oxford University Press, New York.

[Parr et al., 1989](#) – Parr R.G., Yang W. (1989). Density-functional Theory of Atoms and Molecules. Oxford University Press, New York/Oxford.

[Pérez et al., 2009](#) – Pérez P., Domingo L.R., Duque-Noreña M., Chamorro E. (2009). A condensed-to-atom nucleophilicity index. An application to the director effects on the electrophilic aromatic substitutions. *J. Mol. Struct. (Theochem)*, 895: 86-91.

[Rauk et al., 1994](#) – Rauk A. (1994). Orbital interaction theory of organic chemistry”, Wiley, New York.

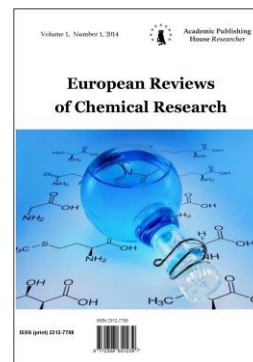
[Waschbüsch et al., 1996](#) – Waschbüsch R., Carran J., Savignac P. (1996). A Convergent Triflate Displacement Approach to (Monofluoroalkyl)phosphonates. *Tetrahedron*, 52: 14199-14216.

Copyright © 2019 by Academic Publishing House Researcher s.r.o.



Published in the Slovak Republic
European Reviews of Chemical Research
Has been issued since 2014.
E-ISSN: 2413-7243
2019, 6(1): 12-22

DOI: 10.13187/erchr.2019.1.12
www.ejournal14.com



Quantum Mechanical Descriptors of Indazole-Containing Derivatives Using the DFT Method

H. Essassaoui^a, M. El idrissi^{a, *}, R. Bouhdadi^a, M. Echajia^a, A. Zeroual^b, A. Tounsi^a, M. Mbarki^a

^a Sultan Moulay Slimane University, Morocco

^b Chouaïb Doukkali University, El Jadida, Morocco

Abstract

Indazole-containing derivatives represent one of the most important heterocycles in drug molecules. Diversely substituted indazole derivatives bear a variety of functional groups and display versatile biological activities; hence, they have gained considerable attention in the field of medicinal chemistry. In this paper, 1H-Indazole and 2H- indazole are optimized by B3LYP/6-311G (d,p) level of theory and ionization potential (IP), electron affinity (EA), and other MDs are determined. Further, non-linear optical (NLO) descriptors such as dipole moment (DM) and polarizability (α) are also determined.

Keywords: Indazole, DFT, NLO, electron affinity, ionization potential, dipole moment, polarizability and thermodynamic properties.

1. Introduction

The nitrogen-containing heterocycles are important building blocks for many bioactive natural products and commercially available drugs. As pharmacologically important scaffolds, they have attracted considerable attention from chemists (Gao, et al., 2016). Indazoles are one of the most important classes of nitrogen-containing heterocyclic compounds bearing a bicyclic ring structure made up of a pyrazole ring and a benzene ring. Indazole usually contains two tautomeric forms: 1H-indazole and 2H- indazole (Figure 1). Since 1H-indazole is more thermodynamically stable than 2H-indazole, it is the predominant tautomer (Teixeira, et al., 2006).

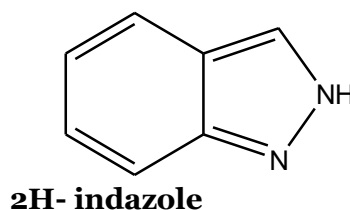
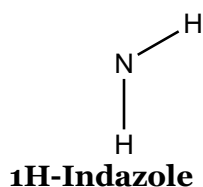


Fig. 1. Indazole nucleus

Indazole derivatives scarcely occur in nature but this particular nucleus in a variety of synthetic compounds possesses a wide range of pharmacological activities, such as anti-

* Corresponding author

E-mail addresses: idrissi_82@hotmail.fr (M. El idrissi)

inflammatory, antiarrhythmic, antitumor, antifungal, antibacterial, and anti-HIV activities (Vidyacharan et al., 2016; Shinde et al., 2016; Behrouz et al., 2017; Jayanthi et al., 2017; Popowycz et al., 2018; Bogonda et al., 2018).

Diversely substituted indazole-containing compounds furnished with different functional groups represent significant pharmacological activities and serve as structural motifs in drug molecules. For example, Bendazac and Benzydamine are two commercially available anti-inflammatory drugs that contain the 1H-indazole scaffold (Figure 2) (Al-Bogami et al., 2016).

There are some excellent reviews that have been published on the biological properties of this class of compounds (Chapolikar et al., 2015; Wang et al., 2018; Tang et al., 2018). This review serves as a comprehensive overview of recent literature that references the synthesis and biological activities of novel indazole-containing derivatives.

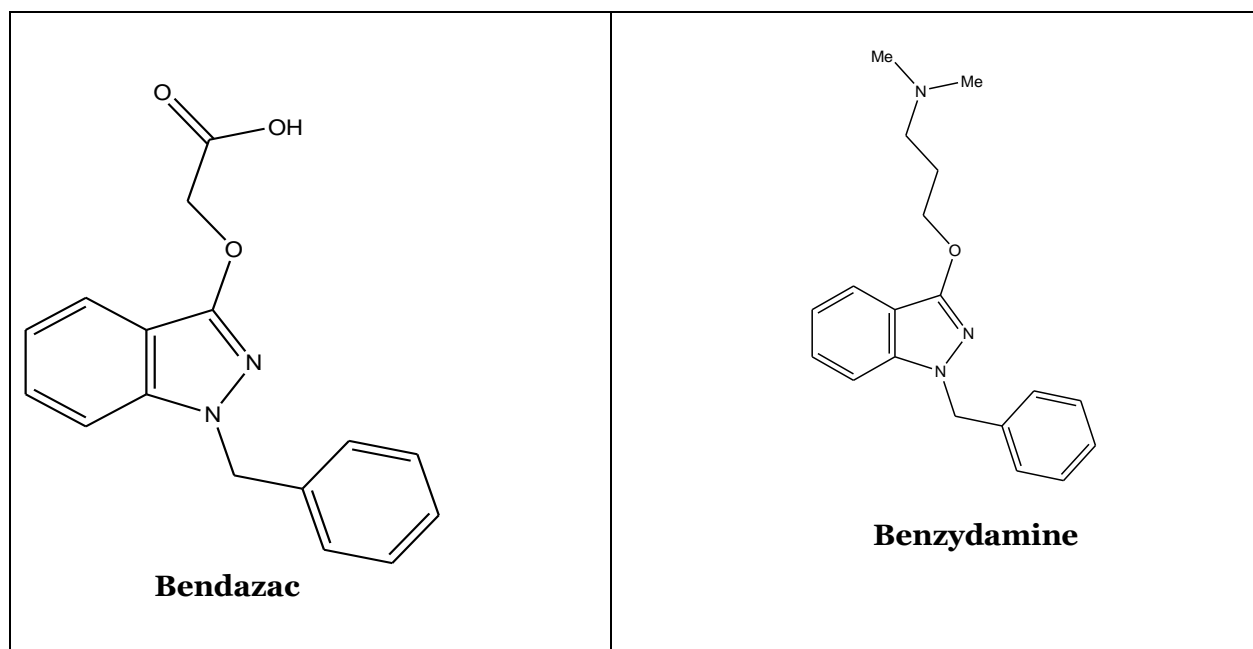
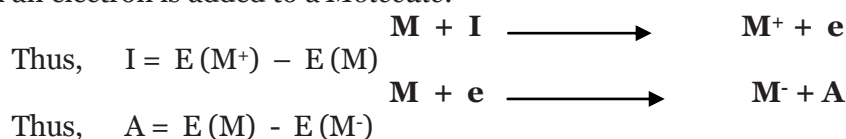


Fig. 2. Chemical structure of indazole-containing drugs

2. Computational methods

Gaussian 09 revision-B. 01-SMP (Wang et al., 2018) and Gauss View 5.0.9 (Chapolikar et al., 2015; Tang et al., 2018) are used as Earlier (Bandyopadhyay et al., 2017) for all computations. Structures were drawn in GAUSS VIEW 5.0.9 [11] of GAUSSIAN (Wang et al., 2018) software package. Initial structures were cleaned repeatedly to obtain normalized geometry. Each of the P1 and P2 was then subjected for successive optimization using semi-empirical (PM3), Hartree–Fock, and DFT methods in conjunction with appropriate basis sets. Final optimization of these molecules is achieved using DFT/B3LYP/6-311G (d, p) method. For computation of linear and NLO properties, the additional key of “optical” was included in the study. Following equations are used for the extraction of parameters and properties of these products. HOMO and LUMO energies are directly extracted from the LOG file of the corresponding optimized structure. The following formula is then used to obtain other dependent QM parameters. IP is the amount of energy required to take away one electron from a neutral molecule (M) and EA , oppositely, is the amount of energy released when an electron is added to a *Molecule*.



μ is the ability of a molecule to participate in the chemical reaction. It can either be positive or negative. It is one of the very important parameters for the determination of the reactivity nature of a molecule. It is referred to as negative of electronegativity (χ) which is estimated as:

$$\mu = -\left(\frac{\delta E}{\delta N}\right)_v = -\left(\frac{\delta E}{\delta \rho}\right)_v = -\left(\frac{I+A}{2}\right); \chi = \left(\frac{I+A}{2}\right)$$

η is a very important parameter that allows understanding of the chemical reactivity of a molecule. It is the slope of the curve of μ , in electronic energy (E) versus electron number plot. In other words, η is the curvature of the μ curve. The value is always positive. However, lower the value, the higher the reactivity of the molecule. η and its reciprocal (i.e., σ) are computed as:

$$\eta = \frac{1}{2}\left(\frac{\delta c}{\delta N}\right)_v = \frac{1}{2}\left(\frac{\delta^2 E}{\delta N^2}\right) = \left(\frac{I-A}{2}\right); \sigma = \frac{1}{\eta}$$

Global electrophilicity index (ω) has been worked out [8] using the μ and η parameters.

$$\omega = \frac{\mu^2}{2\eta}$$

While dipole moment (DM) is the measure of α of a molecule in its ground state, α is the intrinsic capacity of a molecule of having a dipole when it is assaulted with an external electric field. If a molecule is present in a weak, static electric field (of strength, F), then the total energy (E) of the molecule can be express as a Taylors series.

$$E_F = E_0 - \mu_\alpha F_\alpha - \frac{1}{2!}\alpha_{\alpha\beta} F_\alpha F_\beta - \frac{1}{3!}\alpha_{\alpha\beta\gamma} F_\alpha F_\beta F_\gamma - \frac{1}{4!}\alpha_{\alpha\beta\gamma\delta} F_\alpha F_\beta F_\gamma F_\delta - \dots$$

E_0 denotes the energy of the molecule in the absence of an external electrical field. Energy (E_0), dipole moment ($\mu\alpha$), polarizability ($\alpha_{\alpha\beta}$), and first- and second-order hyperpolarizability ($\beta_{\alpha\beta\gamma}$ and $\gamma_{\alpha\beta\gamma\delta}$, respectively) denote the molecular properties. First polarizability and second hyperpolarizabilities are expressed as tensor quantities, whereas subscripts single, double, etc., denote the first-rank and second-rank tensor, etc., in Cartesian coordinate.

If the external field lies on any one of the three orthogonal Cartesian axes, then the components of the induced moments will be parallel to the field. In that case, off-diagonal terms of the tensor, $\alpha_{\alpha\beta}$ vanish. Under this conditions, the expected value of α and DM obtained as:

$$\text{DM} = \sqrt{(\mu_x^2 + \mu_y^2 + \mu_z^2)}$$

$$\text{Or } \langle \alpha_{\text{STATIC}} \rangle = \frac{(\alpha_{xx} + \alpha_{yy} + \alpha_{zz})}{3}$$

In case of the anisotropic orientation of the external field, the anisotropy of the polarizability ($\langle \Delta\alpha \rangle$) can be computed as:

$$\langle \Delta\alpha \rangle = \left[\frac{(\alpha_{xx} - \alpha_{yy})^2 + (\alpha_{yy} - \alpha_{zz})^2 + (\alpha_{yy} - \alpha_{zz})^2 + 6(\alpha_{xy}^2 + \alpha_{xy}^2 + \alpha_{yz}^2)}{2} \right]^{\frac{1}{2}}$$

Similarly, the first-order ($\beta_{\alpha\beta\gamma}$) and second-order ($\gamma_{\alpha\beta\gamma\delta}$) hyperpolarizability is calculated from components of respective tensors that are obtained from the GAUSSIAN output file.

$$\langle \beta_{\text{STATIC}} \rangle = \left[\beta_x^2 + \beta_y^2 + \beta_z^2 \right]^{\frac{1}{2}}$$

$$\beta_i = \beta_{iii} + \frac{1}{3} \sum_{i \neq k} (\beta_{ikk} + \beta_{kik} + \beta_{kki})$$

$$\langle \beta_{\text{STATIC}} \rangle = \left[(\beta_{xxx} + \beta_{xyy} + \beta_{xzz})^2 + (\beta_{yyy} + \beta_{yzz} + \beta_{yxx})^2 + (\beta_{zzz} + \beta_{zxx} + \beta_{zyy})^2 \right]^{\frac{1}{2}}$$

$$\langle \gamma_{STATIC} \rangle = \frac{\gamma_{XXXX} + \gamma_{YYYY} + \gamma_{ZZZZ} + 2\gamma_{YYXX} + 2\gamma_{YYZZ} + 2\gamma_{ZZXX}}{5}$$

All these optical terms have been calculated using appropriate basis set that contains polarized and diffused functions for high accuracy, in that DFT/B3LYP/6-311G(d,p) was preferred.

3. Results and discussion

3.1. Bond length and angle properties

Quantum mechanically optimized structures are shown in [Figure 2](#). The seared used to determine selective bond lengths (in Å) and angles (in degree), the result of which are presented in [Tables 1](#) and [2](#), respectively, along with available experimental results for comparison purposes. Common atoms in the structures of these products are identified using an arbitrary numbering scheme ([Figure 1](#)). Bendazac (P1) and Benzydamine (P2). Following points are noteworthy from these tables.

First, common bond lengths are almost identical ([Table 1](#)) for these impurities (P1 and P2), that show variations (underlined: [Table 1](#)) when compared with that of itself ([Table 1](#)). Notable, due to lack of P1 and P2, last four bond lengths are not available for comparison purpose. Second, similar to bond lengths, relevant angles are also compared in [Table 2](#). It is seen that product shows slight variations in few of its representative angles when compared with that of the impurities. However, these impurities show remarkable similarities in angles when compared among themselves.

Table 1. Bond lengths (in Å) of Bendazac and Benzydamine. (The experimental values of the former are extracted from the crystal structure ([Johnston et al., 1998](#))).

Bond length in Å	Bendazac	Exp(Crystal)	Benzydamine	Exp(Crystal)
C-C	1.380	1.369	1.445	1.435
C-N	1.457	1.413	1.470	1.458
C-O	1.430	1.398	1.430	1.412
C=C	1.445	1.457	1.404	1.466
N-N	1.407	1.395	1.407	1.423
O-H	1.430	1.496	1.431	1.511

Table 2. Angles (in Å) of Bendazac and Benzydamine . (The experimental values of the former are extracted from the crystal structure ([Johnston et al., 1998](#))).

Angles in Å	Bendazac	Exp(Crystal)	Benzydamine	Exp(Crystal)
C-C-C	109.469	109.587	109.471	109.589
C-O-H	109.502	109.688	109.607	109.654
C-N-N	159.017	160.021	109.572	109.687
C-N-C	109.487	109.657	109.471	109.566
O=C-O	109.471	109.568	109.459	109.756
C=C-C	118.452	119.112	121.138	120.987
H-C-H	109.471	109.789	109.471	110.012
C=C-H	120.270	121.021	119.111	120.231

3.2. Optimized structure, electronic parameters and properties

The highest occupied molecular orbital (HOMO) and lowest unoccupied molecular orbital (LUMO) for Bendazac (P1) and Benzydamine (P2) are presented in [Figure 1](#), along with their optimized structures. While HOMO delocalizes over bonds of P1, and P2, it is less prominent for P1 and P2. Notably, the delocalization is uniform in P1. By the use of DFT/B3LYP/6-311G(d,p) level of theory, the extracted energies for HOMO, LUMO, and ΔE for P1 and P2 are presented in [Table 3](#).

Table 3. HOMO, LUMO, and band gap energies for P1 and P2 (HOMO and LUMO are directly extracted from the LOG file of the Gaussian optimized structure. The band gap is computed by $E_{\text{LUMO}} - E_{\text{HOMO}}$)

Molecule	HOMO (eV)	LUMO (eV)	Band gap (eV)
Bendazac	-6.004	-3.305	2.698
Benzydamine	-3.431	-0.581	2.849

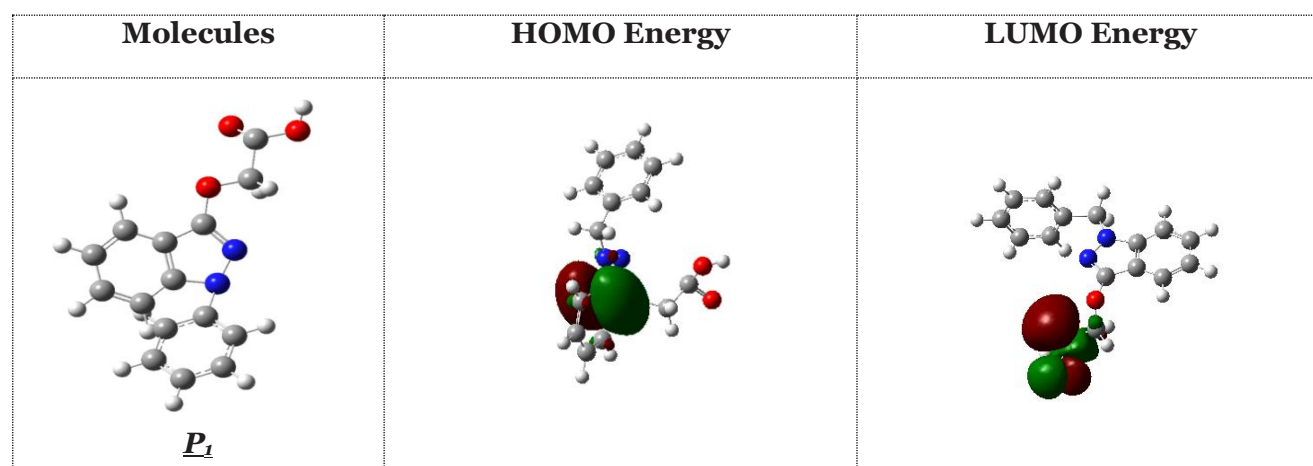
We have computed adiabatic **IP** and adiabatic **EA** for P1 and P2 and presented in Table 4. Value deviates from the mean value are highlighted by underline. **IP**: Ionization potential, **EA**: Electron affinity, **μ** : Chemical potential, **χ** : Electronegativity, **η** : Chemical hardness, **σ** : Chemical softness ($1/\eta$), **ω** : Electrophilicity index.

*Mean of IP and EA is 7.5 eV and 0.4 eV, respectively (Schipper et al., 2000).

Table 4. Computation of electron affinity, ionization energy, chemical potential, electronegativity, chemical hardness, chemical softness, and electrophilicity index for P1 and P2 products

<i>All Molecule units are in (eV)</i>							
Molecule	IP	EA	M	X	η	σ	ω
P1	6.004	3.305	-4.654	4.654	2.699	0.370	4.012
P2	3.431	0.581	-2.006	2.006	2.849	0.351	0.706

The highest occupied molecular orbital (HOMO) and lowest unoccupied molecular orbital (LUMO) for P1 and P2 are presented in Figure 3, along with their optimized structures. While HOMO delocalizes over bonds of P1 and P2, it is less prominent of P1 and P2. Notably, the delocalization is uniform in P1. In turn, the LUMO is mostly located for P1 and P2. By the use of DFT/B3LYP/6-311G (d,p) level of theory.



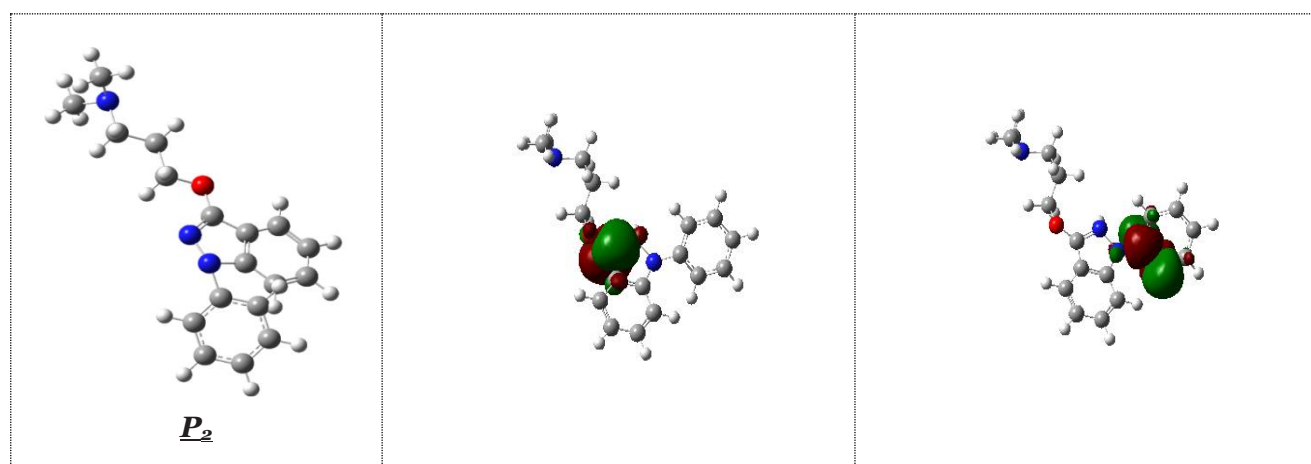


Fig. 3. Energy optimized structures (left column) along with highest occupied molecular orbitals (middle panel) and lowest unoccupied molecular orbitals (right panel) or frontier molecular orbitals of P1 and P2

The [Table 4](#) shows that IP of P1 is higher than IP of P2. Here, P1 is seen to be anomalously high and P2 almost similar as the mean value of normal drugs ([Bogonda et al., 2018](#)). High *IP* implies low tendency for the formation of the cation. On the other hand, higher the *EA*, greater is the tendency for the formation of an anion. Although, the mean value of *EA* for normal drugs is ~ 0.6 eV, the possess high P2 and low (for P1) values of *EA*, μ , χ , η , σ , and electrophilicity index (ω) properties are also presented in [Table 4](#). All these properties are dependable on *IP* and *EA*. It is seen that ω value follows the similar order as *EA*, $P1 > P2$.

3.3. Non-linear optical (NLO) of P1 and P2

Intermolecular interactions such as drug-protein/DNA/RNA are largely understood by DM, α , and first-order and second-order hyperpolarizability energy terms ([Hurst et al., 1998](#)), which are reliably computed by RB3LYP/6-311G (d,p) level of the theory ([Bandyopadhyay et al., 2017](#)). How are these parameters affected for P1 and P2. To check this above basis set is used and dipole moments (DM), α , and first- and second-rank hyperpolarizability are determined. Isotropic DM is presented in [Table 5](#).

Table 5. Cartesian components and net electric dipole moments (*DM* in Debye) for P1 and P2

Names	<i>DM_x</i>	<i>DM_y</i>	<i>DM_z</i>	<i>DM_{Total}</i>
P₁	0.965	-3.257	-2.437	4.181
P₂	2.439	-1.665	-1.412	3.274

It is seen that the X and Y components are zero in all the cases with the Z component constituting the total *DM*. Higher and lower *DM_{TOTAL}* than the reported mean value are highlighted by the [Table 6](#). Here, P1 and P2 show higher and lower *DM_{TOTAL}*, respectively.

Molecular complexity is the criterion that can be related with $\Delta\alpha$ ([Chen et al., 2017](#); [Aihara et al., 1999](#); [Obot et al., 2009](#); [Ghanadzadeh et al., 2000](#); [Zhan et al., 2003](#); [Xue et al., 2004](#); [Xue et al., 1999](#); [Lim et al., 1999](#); [Hansch et al., 2003](#); [Boger et al., 2003](#); [Lee et al., 2001](#)). More the complexity of structure more is the anisotropy of polarizability ($\Delta\alpha$).

*Higher and lower values are underlined with respect to the mean of α , which is 34×10^{-24} esu ([Schipper, et al., 2000](#)).

Table 6. Components and mean isotropic (α) and anisotropic ($\Delta\alpha$) polarizability (in 10^{-24} esu unit) for P1 and P2

Name	α_{xx}	α_{yx}	α_{yy}	α_{zx}	α_{zy}	α_{zz}	α	$\Delta\alpha$
P ₁	18.734	-4.053	21.054	-7.503	-3.174	27.253	12.343	17.506
P ₂	22.175	2.214	18.467	-5.719	3.468	21.287	20.646	12.628

α , its components, and anisotropic terms are shown in Table 6. The α of P1 is seen to be much lower than α in P2 case. In these aspects, P2 is seen to be less affected (Table 6). Similar is the case for the anisotropy of polarizability ($\Delta\alpha$) and diagonal components of polarizability (α_{xx} , α_{yy} , and α_{zz}), where P1 have much lower value than P2. Is there any relation of α with chemical reactivity.

If molecular hardness and softness are compared with the α profile (Table 4), we see that it is inversely and directly relation with the α (Table 6), respectively. Which of the three P1 is most polarizable and which one is most active chemically.

It is seen that P1 is mor polarizable than P2. It is also seen that it possesses lowest hardness and highest softness. Interestingly, the anisotropy of α of P2 is also higher than P1.

3.4. Molecular electrostatic potential and reactivity for title compounds

The electron density is considered a very important factor for understanding the reactivity of electrophilic and nucleophilic sites and the interactions of hydrogen bonding (Gresh et al., 2007; Scrocco et al., 1979; Luque et al., 2000), as well as this density, is related to the molecular electrostatic potential (MEP). Therefore for predicting this reactivity of nucleophilic and electrophilic sites attacks for studied compounds, we simulated the MEP of these compounds using the B3LYP level of the optimized geometry. The different colors (red, blue and green) at the MEP surface represent different values of the electrostatic potential as the regions of most negative, most positive and zero electrostatic potential respectively. The negative electrostatic potential at the MEP (shades of red) indicates that this region is attractive of the proton by the aggregate electron density in the molecule, while the positive electrostatic potential (shade of blue) is the region that presents of the repulsion of the proton by the atomic nuclei. The negative regions at MEP (red) correspond to electrophilic reactivity (regions of most electronegative electrostatic potential) and the positive region(blue) correspond to nucleophilic reactivity (regions of the most positive electrostatic potential) and green represent regions of zero potential.

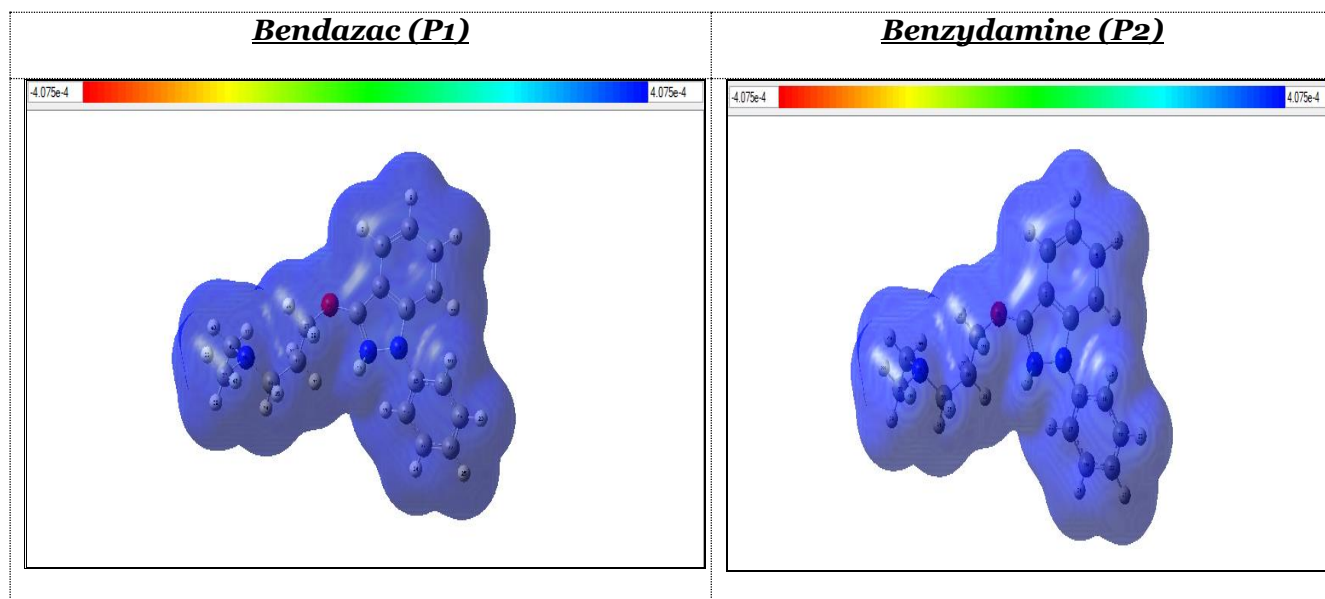


Fig. 4. Calculated electrostatic potential surfaces on the molecular surfaces of studied compounds P1 and P2. (Color ranges, in kcal/mol: from red -4.075×10^{-4} to blue $+4.075 \times 10^{-4}$ B3LYP functional and 6-311G (d,p) basis set)

3.3. Thermodynamic properties

Computation of thermodynamic properties of P1 and P2 products is important for both thermochemistry and chemical equilibrium. Statistical thermodynamics with the two key ideas, Boltzmann distribution and the partition function leads to the derivation of the equations utilized for computing thermochemical enthalpy (ΔH^0), dipole moment and the rotational constants of the molecular system were obtained directly from the output of Gaussian calculation employing B3LYP/6-311G(d,p) basis set and are listed in the Tables 7a, 7b and 7c.

Table 7a. Variation of different thermodynamic parameters with temperature (Bendazac P1)

Temperature (K)	Enthalpy ΔH (Kcal/mol)	Entropy ΔS (Cal/mol.K)	Specific heat C_p (Cal/mol.K)
100	-588.841	159.218	34.215
200	-586.326	162.354	39.124
300	-581.023	163.897	42.147
400	-576.236	165.027	45.678
500	-571.056	169.874	49.785
600	-562.453	171.236	51.013
700	-559.367	175.965	52.698
800	-550.259	177.889	55.234

Table 7b. Variation of different thermodynamic parameters with temperature (Benzydamine P2)

Temperature (K)	Enthalpy ΔH (Kcal/mol)	Entropy ΔS (Cal/mol.K)	Specific heat C_p (Cal/mol.K)
100	-598.075	126.459	36.458
200	-596.245	130.256	39.789
300	-594.879	135.789	43.012
400	-591.023	131.671	46.358
500	-585.214	128.369	50.247
600	-581.789	123.458	53.697
700	-575.984	120.444	55.489
800	-570.325	117.885	59.782

Table 7c. Different thermodynamic parameters at room temperature (P1 and P2)

Parameters	B3LYP/6-311G (d,p)	
	Bendazac (P1)	Benzydamine (P2)
Total energy (Hartree)	-953,105	-938,389
Zero-point vibrational energy (Kcal/mol)	167,546	231,903
Rotational constants (GHz)	0,465	0,564
	0,548	0,621
	0,789	0,879

The correlation between temperature and these thermodynamic properties are given by Figure 5. The correlation equations are as follows:

$$H_m^0 = -599.3586 - 0.0389 T - 9.2154 \cdot 10^{-4} T^2 \quad (R^2 = 0.9145)$$

$$S_m^0 = 121.337 + 0.3547 T - 5.3214 \cdot 10^{-4} T^2 \quad (R^2 = 0.9575)$$

$$C_{p,m}^0 = 1.2574 + 0.2447 T - 3.2248 \cdot 10^{-4} T^2 \quad (R^2 = 0.9715)$$

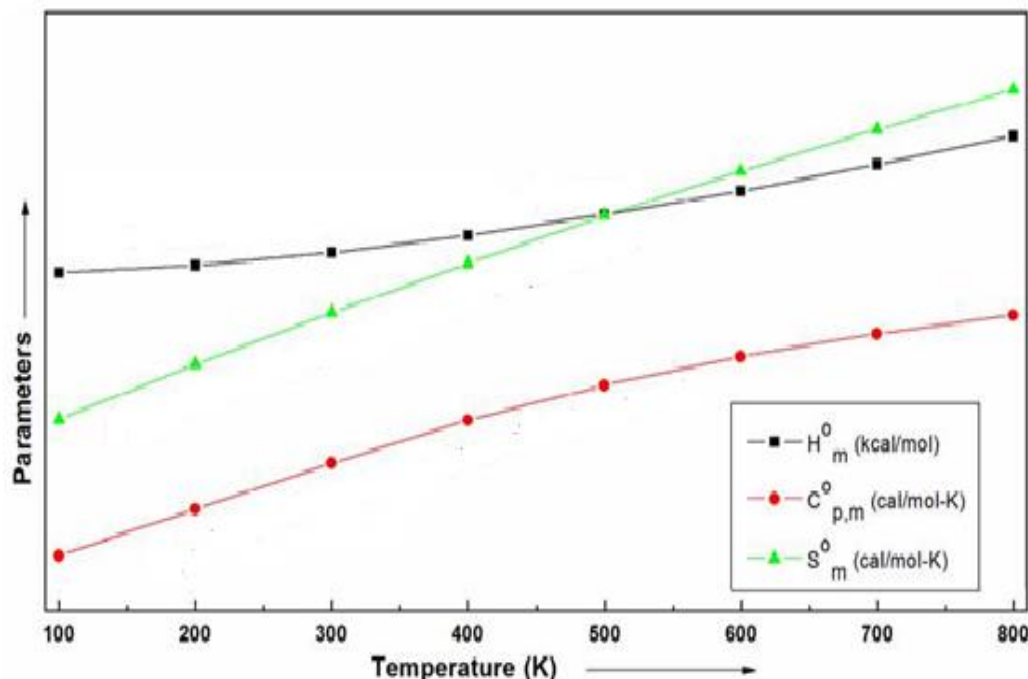


Fig. 5. Correlation between different thermodynamic properties with the temperature

It is observed that the parameters increase from 100 to 800 K due to the increase in the molecular vibrational intensities with the temperature.

4. Conclusion

Electronic structural properties for representative the P1 and P2 products are worked out by RB3LYP/6-311G (d, p) level of theory of Gaussian 09 software package. The ground state optimized structures are used for computation of electronic and NLO properties. Corresponding bond lengths and angles of these products show remarkable similarity among themselves but show variation.

The observation of high EA , low band gap, low η , high χ , and high IP of P1 may indicate that it is strongly electrophilic in nature.

P1 product more polarizable, hyperpolarizable and chemically more reactive compared to P2. So P1 it is more interactive to target molecule.

5. Conflict of Interest

The authors declare that there is no conflict of interests regarding the publication of this paper. Also, they declare that this paper or part of it has not been published elsewhere.

6. Acknowledgments

The authors are thankful for Laboratory of Chemical Process and Applied Materials. Sincere thanks are also due for Prof. Mohamed Mbarki, Department of Chemistry and Environment, Faculty of Science and Technologies, Sultan Moulay Slimane University, Morocco, for valuable comments for the manuscript.

References

AI-Bogami et al., 2016 – AI-Bogami A.S. (2016). Mechano chemical synthesis of cyclohexenones and indazoles as potential antimicrobial agents. *Res. Chem. Intermed.*, 42, 5457-5477.

Aihara et al., 1999 – Aihara JI. (1999). Reduced HOMO-LUMO gap as an index of kinetic stability for polycyclic aromatic hydrocarbons. *J Phys Chem A.*, 103: 7487-95.

Bandyopadhyay et al., 2017 – Ansary I., Das A., Gupta P.S., Bandyopadhyay A.K. (2017). Synthesis, molecular modeling of N-acyl benzoazetinones and their docking simulation on fungal modeled target. *Synth Commun*, 47: 1375-86.

Behrouz et al., 2017 – Behrouz S. (2017). Highly efficient one-pot three component synthesis of 2H-indazoles by consecutive condensation, C-N and N-N bond formations using Cu/Aminoclay/reduced graphene oxide nanohybrid. *J. Heterocyclic. Chem.*, 54, 1863-1871.

Boger et al., 2003 – Boger DL., Desharnais J., Capps K. (2003). Solution-phase combinatorial libraries: Modulating cellular signaling by targeting protein-protein or protein-DNA interactions. *Angew Chem Int Ed Engl.*, 42: 4138-76.

Bogonda et al., 2018 – Bogonda G., Kim H.Y., Oh K. (2018). Direct acyl radical addition to 2H-indazoles using Ag-catalyzed decarboxylative cross-coupling of α -keto acids. *Org. Lett.*, 20, 2711-2715.

Chapolikar et al., 2015 – Gaikwad DD, Chapolikar AD, Devkate CG, Warad KD, Tayade AP, Pawar RP, Domb AJ. (2015). Synthesis of indazole motifs and their medicinal importance: An over view. *Eur. J. Med. Chem.*, 90, 707-731.

Chen et al., 2017 – Chen L., Lu J., Huang T., Cai YD. (2017). A computational method for the identification of candidate drugs for non-small cell lung cancer. *PLoS One*, 12: e0183411.

Gao et al., 2016 – Gao M., Xu, B. (2016). Transition metal-involving synthesis and utilization of N-containing heterocycles: Exploration of nitrogen sources. *Chem. Rec.*, 16, 1701-1714.

Ghanadzadeh et al., 2000 – Ghanadzadeh A., Ghanadzadeh H., Ghasmi G. (2000). On the molecular structure and aggregative properties of Sudan dyes in the anisotropic host. *J Mol Liq.*, 88: 299-308.

Gresh et al., 2007 – Cisneros GA., Darden TA., Piquemal JP. (2007). Anisotropic, polarizable molecular mechanics studies of inter- and intramolecular interactions and ligand-macromolecule complexes. A Bottom-up strategy. *J. Chem Theory Comput.*, 3: 1960-86.

Hansch et al., 2003 – Hansch C., Steinmetz WE, Leo AJ, Mekapati SB, Kurup A, Hoekman D. (2003). On the role of polarizability in chemical-biological interactions. *J. Chem Inf Comput Sci.*, 43: 120-125.

Hurst et al., 1998 – Hurst GJ., Dupuis M., Clementi E. (1998). A binitio analytic polarizability, first and second hyperpolarizabilities of large conjugated organic molecules: Applications to polyenes C₄H₆ to C₂₂H₂₄. *J. Chem Phys.*, 89: 385-95.

Jayanthi et al., 2017 – Jayanthi M., Rajakumar P. (2017). Synthesis, cell viability, and flow cytometric fluorescence pulse width analysis of dendrimers with indazoles surface unit. *J. Heterocyclic. Chem.*, 54, 3042-3050.

Johnston et al., 1998 – Harris K.D.M., Johnston R.L., Kariuki B.M. (1998). Acta Crystallogr. Sect. A: Found. *Crystallogr*, 54: 632-645.

Lee et al., 2001 – Lee JY, Kim KS, Mhin BJ. (2001). Intramolecular charge transfer of π -conjugated push-pull systems in terms of polarizability and electronegativity. *J. Chem Phys.*, 115: 9484-9.

Lim et al., 1999 – Lim I.S., Pernpointner M., Seth M., Laerdahl J.K., Schwerdtfeger P., Neogrady P. (1999). Relativistic coupled-cluster static dipole polarizabilities of the alkali metals from Li to element 119. *Phys Rev A.*, 60: 2822.

Luque et al., 2000 – Luque F.J., Lopez J.M., Orozco M. (2000). Perspective on electrostatic interactions of a solute with a continuum. A direct utilization of ab initio molecular potentials for the prevision of solvent effects. *Theor. Chem. Acc.*, 103, 343-345.

Obot et al., 2009 – Obot IB., Obi-Egbedi NO., Umoren SA. (2009). Antifungal drugs as corrosion inhibitors for aluminium in 0.1 M HCl. *Corrosion Science*, 51(8): 1868-75.

Popowycz et al., 2018 – Laurard H., Popowycz F. (2018). Regioselective late-stage C-3-functionalization of pyrazolo-[3,4-b]pyridines. *Synthesis*, 50, 998-1006.

Schipper et al., 2000 – Schipper PR, Gritsenko OV, Van Gisbergen SJ, Baerends EJ. (2000). Molecular calculations of excitation energies and (hyper) polarizabilities with a statistical average of orbital model exchange-correlation potentials. *J. Chem Phys.*, 112: 1344-1352.

Scrocco et al., 1979 – Scrocco E., Tomasi J. (1979). Electronic molecular structure, reactivity and intermolecular forces: an heuristic interpretation by means of electrostatic molecular

potentials, *Adv. Quantum Chem.*, 1, 115-121.

[Shinde et al., 2016](#) – *Shinde A., Vidyacharan H.S., Sharada D.S.* (2016). BF₃-OEt₂ mediated metal-free one-pot sequential multiple annulation cascade (SMAC) synthesis of complex and diverse tetrahydro isoquinoline fused hybrid molecules. *Org. Biomol. Chem.*, 14, 3207-3211.

[Tang et al., 2018](#) – *Wan Y.C., He S.Z., Li W., Tang Z.L.* (2018). Indazole derivatives: Promising anti-tumor agents. *Anti-Cancer Agents. Med. Chem.*, 18, DOI: 10.2174/1871520618666180510113822

[Teixeira et al., 2006](#) – *Teixeira F.C., Ramos H., Antunes I.F., M. João M. Curto, Teresa Duarte M., Bento I.* (2006). Synthesis and structural characterization of 1- and 2-substituted indazoles: Ester and carboxylic acid derivatives. *Molecules*, 11, 867–889.

[Vidyacharan et al., 2016](#) – *Vidyacharan S., Murugan A., Sharada D.S.* (2016). C(sp²)-H Functionalization of 2H-indazoles at C₃-position via palladium(II)-catalyzed isocyanide insertion strategy leading to diverse heterocycles. *J. Org. Chem.*, 81, 2837-2848.

[Wang et al., 2018](#) – *Dong J.Y., Zhang Q.J., Wang Z.T., Huang G., Li S.S.* (2018). Recent advances in the development of indazole-based anticancer agents. *Chem. Med. Chem.*, 13, 1490-1507.

[Xue et al., 1999](#) – *Harris P.G., Baker C.A., Green K., Iaydjiev P., Ivanov S.I., May D.J.* (1999). New experimental limit on the electric dipole moment of the neutron. *Phys Rev Lett.*, 82: 904.

[Xue et al., 2004](#) – *Xue Y., Li ZR., Yap CW., Sun LZ., Chen X., Chen YZ.* (2004). Effect of molecular descriptor feature selection in support vector machine classification of pharmacokinetic and toxicological properties of chemical agents. *J Chem Inf Comput Sci.*, 44: 1630-8.

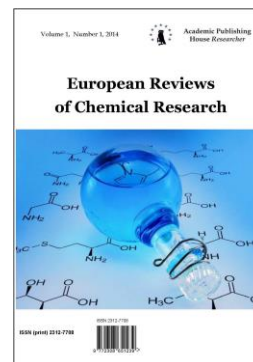
[Zhan et al., 2003](#) – *Zhan CG, Nichols JA, Dixon DA.* (2003). Ionization potential, electron affinity, electronegativity, hardness, and electron excitation energy: Molecular properties from density functional theory orbital energies. *J. Phys Chem A.*, 107: 4184-95.

Copyright © 2019 by Academic Publishing House Researcher s.r.o.



Published in the Slovak Republic
European Reviews of Chemical Research
Has been issued since 2014.
E-ISSN: 2413-7243
2019, 6(1): 23-28

DOI: 10.13187/erchr.2019.1.23
www.ejournal14.com



Experimental and Theoretical Elaboration of Phase Diagram for the Ternary System $\text{Ni}(\text{NO}_3)_2$ - $\text{Al}(\text{NO}_3)_3$ - H_2O at 20°C

M. Jouaiti ^a, B. Mekkaoui ^a, A. Barroug ^a, M. El idrissi ^{a, b, *}, R. Lbibb ^a, L. Lâallam ^a, A. Jouaiti ^a

^a Sultan Moulay Slimane University, Morocco

^b Chouaib Doukkali University, El Jadida, Morocco

Abstract

The solid-liquid equilibrium of the ternary system of H_2O - $\text{Al}(\text{NO}_3)_3$ - $\text{Ni}(\text{NO}_3)_2$ were studied using a synthesis process based on conductivity measurements. The isotherm was experimentally established at a 30°C . The aim of our work is to validate the results obtained experimentally by an algorithm based on the Pitzer equations as well as the Nelder-Mead simplex method, which is an optimization method for multivariate function. A comparison between the obtained isotherm from the experimental data and the elaborated one using Pitzer model has confirmed our results.

Keywords: Pitzer model, solubility isotherms, $\text{Al}(\text{NO}_3)_3$ - $\text{Ni}(\text{NO}_3)_2$ - H_2O .

1. Introduction

A phase diagram is a thermodynamic tool, allowing after its analysis to give us a deep description about what happens at the microscopic level in the studied system. The liquid-solid phases equilibrium diagrams based on water and metal nitrates were the subject of many previous studies due to their properties, which give them opportunities for interesting industrial applications, especially for the synthesis of bi- or tri-metallic oxides (Goundali et al., 2006). Indeed Solubility equilibrium between solid salts, salt hydrates and water play an important role in different branches of applied chemistry such as, hydrometallurgy, geochemistry and oceanography, Hence thermodynamic models can be powerful predictive and interpretive tools to study the geochemistry of natural waters and mineral deposits, solve environmental problems and optimize industrial processes; indeed the Pitzer model is one of the most used ones, which has enjoyed remarkable success. It is especially popular with geochemists, waste chemists, and engineers for prediction of mineral solubilities and phase equilibrium.

2. Experimental work

Conductivity measurements were the basic synthetic method for the determination of solubility curves (Tenu et al., 1973; Kaddami et al., 1986; Tenu et al., 1979). It consists practically, in adding small amounts of water to the saturated solution in order to toggle it from its equilibrium state. Once the new equilibrium is restored after the addition of the water, the conductivity is measured and it is represented in terms of the quantity of added water (Laallam et al., 2004; Laallam et al., 2003; Laallam et al., 2011). Then, we follow for a set of poly-phase mixtures (liquid+solid) of the appropriate composition, the variation of the liquid phase conductivity according to

* Corresponding author

E-mail addresses: idrissi_82@hotmail.fr (M.El idrissi)

the dilution of the initial mixture. The electric conductivity-composition curve of solution introduces a discontinuity at each phase change. When the identification of the solid phase was too difficult with the previous method, the components were subjected to the dosage. Initially, salts are the Nickel nitrate with six water molecules and the Aluminum nitrate with nine water molecules. Water has been used bi-distilled.

The phase determination was our second step after the solubility limits definitions for a several mixed solution, indeed the identification of solid phase was a little difficult using conductivity measurements. Hence comes the metering method, which consists to identify the Nickel sulfate and the Aluminum sulfate using the wet residues and the “ensembles” methods (Chretien et al., 2011; Jouaiti et al., 1983; Schreinemakers et al., 1983). The Ni ions have been measured by molecular absorption spectrophotometry, the Al ions by volumetry using the EDTA.

In this study, we adopted definitions and notations of rectangular coordinates, we calculated the weight composition coordinates of considered mixture points by using the following expressions:

$$W(\text{Al}(\text{NO}_3)_3) = 100 * \frac{m(\text{Al}(\text{NO}_3)_3)}{m_t}$$

$$W(\text{Ni}(\text{NO}_3)_2) = 100 * \frac{m(\text{Ni}(\text{NO}_3)_2)}{m_t}$$

$$m_t = m(\text{Al}(\text{NO}_3)_3) + m(\text{Ni}(\text{NO}_3)_2) + m(\text{H}_2\text{O})$$

The experimental isotherm obtained at 20°C, (Jouaiti et al., 1983), is given in Table 1.

Table 1. The measured solubility data of ternary system $\text{Al}(\text{NO}_3)_3 + \text{Ni}(\text{NO}_3)_2 + \text{H}_2\text{O}$ at 20°C

W (Al(NO ₃) ₃),%	W (Ni(NO ₃) ₂),%	Limit domains
0	47.98	Liq+Ni ₆
4.33	43.18	--
8.6	38.1	--
11.2	36.22	AL ₉ + Ni ₆ + Liq
13.11	33.84	Liq+AL ₉
16.9	28.1	--
23.9	17.1	--
30.9	8.5	--
38.37	0	--

The experimental results of the solubility isotherm obtained at 20°C are given in Figure 1.

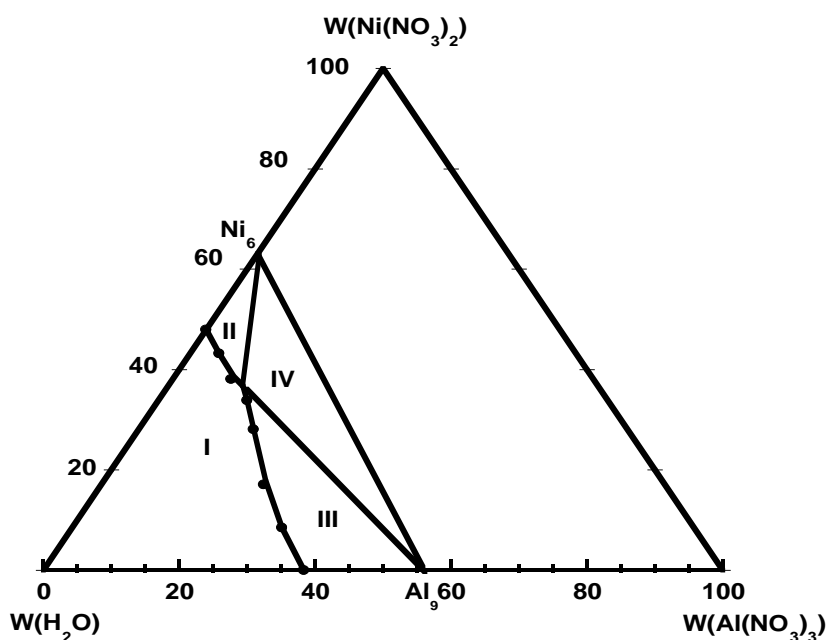


Fig. 1. The 20°C solubility isotherm of $\text{Al}(\text{NO}_3)_3$ - $\text{Ni}(\text{NO}_3)_2$ - H_2O ternary system

3. Page and column layout

The details of ion- interaction have already been discussed in preceding PITZER publication, the following equation 1, 2 and 3 are the main equations employed in our calculations.

$$(\varphi_{osmotic} - 1) = \frac{2}{\sum_i m_i} \left[\begin{aligned} & \frac{-A_\phi I^{\frac{3}{2}}}{(1+bI^{\frac{1}{2}})} + \sum_c \sum_a m_c m_a (B_{ca}^\phi + ZC_{ca}) \\ & + \sum_{c < c'} \sum_c m_c m_{c'} (\phi_{cc'}^\phi + \sum_a m_a \psi_{cc'a}) + \\ & \sum_{a < a'} \sum_a m_a m_{a'} (\phi_{aa'}^\phi + \sum_c m_c \psi_{caa'}) \end{aligned} \right] \quad (1)$$

$$\ln(\gamma_M) = z_M^2 F + \sum_a m_a (2B_{Ma} + ZC_{Ma}) + \sum_c m_c (2\phi_{Mc} + \sum_a m_a \psi_{Mca}) + \sum_{a < a'} \sum_a m_a m_{a'} \psi_{Maa'} + z_M \sum_c \sum_a m_c m_a C_{ca} \quad (2)$$

$$\ln(\gamma_X) = z_X^2 F + \sum_c m_c (2B_{cX} + ZC_{cX}) + \sum_a m_a (2\phi_{Xa} + \sum_c m_c \psi_{cXa}) + \sum_{c < c'} \sum_c m_c m_{c'} \psi_{cc'X} + |z_X| \sum_c \sum_a m_c m_a C_{ca} \quad (3)$$

The summations in Eqs (1), (2) and (3) over c and a respectively are summations over the cations and the anions respectively present in the solution. The various terms in Eqs. (1), (2) and (3) are defined as follows:

$$I = 1/2 \sum_i m_i z_i^2 \quad (4)$$

$$Z = \sum_i m_i |z_i| \quad (5)$$

$$F = f^\gamma + \sum_c \sum_a m_c m_a B'_{ca} + \sum_{c < c'} \sum_c m_c m_{c'} \phi'_{cc'} + \sum_{a < a'} \sum_a m_a m_{a'} \phi'_{aa'} \quad (6)$$

$$f^\gamma = -A_\phi \left[\frac{I^{1/2}}{1+bI^{1/2}} + \frac{2}{b} \ln(1+bI^{1/2}) \right] \quad (7)$$

$$B_{MX} = \beta_{MX}^{(0)} + \beta_{MX}^{(1)} g(\alpha_1 I^{\frac{1}{2}}) + \beta_{MX}^{(2)} g(\alpha_2 I^{1/2}) \quad (8)$$

$$C_{MX} = C_{MX}^\phi / 2 |Z_M Z_X|^{1/2} \quad (9)$$

$$g(x) = 2[1 - (1-x)e^{-x}]/x^2 \quad (10)$$

$$B'_{MX} = \beta_{MX}^{(1)} g'(\alpha_1 I^{\frac{1}{2}}) + \beta_{MX}^{(2)} g'(\alpha_2 I^{1/2}) \quad (11)$$

$$g'(x) = -2[1 - (1 + x + 1/2x^2)e^{-x}]/x^2 \quad (12)$$

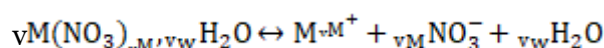
$$\phi_{ij}^{\phi} = \theta_{ij} + {}^E\theta_{ij}(I) + I^E\theta'_{ij} \quad (13)$$

$$\phi_{ij} = \theta_{ij} + {}^E\theta_{ij}(I) \quad (14)$$

$$\phi'_{ij} = {}^E\theta'_{ij}(I) \quad (15)$$

The ion-interaction model gives an equation for the activity and osmotic coefficient of electrolyte solution depending to four binary parameters, $\beta^{(0)}$, $\beta^{(1)}$, $\beta^{(2)}$, C^{ϕ} and two ternary ones ψ and θ . These parameters allow us the calculation of the equilibrium constant of each component in the systems at different temperature.

The solubility of hydrated salt in electrolyte solutions can be calculated from thermodynamic equations. For a hydrated salt, $v_M(\text{NO}_3)_{\cdot v_M} \cdot v_W \text{H}_2\text{O}$, the solubility at a given temperature for the dissolution reaction:



Is given by:

$$K_t = a_{M^+} \cdot (a_{\text{NO}_3^-})^{v_M} \cdot a_w^{v_W}$$

Where a_i and a_w represent respectively the activity of the ion i and water.

$$K_t = m_{M^+} \cdot \gamma_{M^+} \cdot (m_{\text{NO}_3^-} \cdot \gamma_{\text{NO}_3^-})^{v_M} (a_w)^{v_W}$$

Where m_i and γ_i , represent respectively, the molality and the activity coefficient of the ions i . The activity of water is related to the osmotic coefficient (Pitzer et al., 1977) by the given equation:

$$\ln a_w = - \frac{\phi \cdot \sum_i m_i \cdot M_w}{1000}$$

In which:

M_w Represents the molecular mass of water, the sum covers all solute species. Activity and osmotic coefficients are calculated by using the PITZER model (Jouaiti et al., 2017; Pitzer et al., 1977).

4. Theoretical model

In this work, the algorithm used is already established in a previous article (Jouaiti et al., 2018). One of the most basic parts of this algorithm is on finding the Pitzer parameters for a system that we know the experimental data.

The principle is to change the values of these parameters so that it can minimize the objective function, indeed this function is expressed in terms of the difference between the experimental and theoretical values calculated from the Pitzer parameters at each iteration (Jouaiti et al., 2018).

In the following, we will mainly consider the studied ternary system with a common ion, in this case we're facing three binary PITZER parameters which are already known from literature, and two ternary ones which are the aim of the present work. The idea is to calculate the equilibrium constant K_b for the binary system for an initial Pitzer parameters, then, the equilibrium constant K_t for the ternary system is calculated from for all experimental molality data (Jouaiti et al., 2018). At the end, the objective function can be calculated as follow:

$$\sum_{i=1}^N (K_t(m_c, m_{c'}, m_a) - K_b)^2$$

Where:

N: number of data points in the solubility isotherm.

m_c, m_{c}' : experimental molality of cation.

m_a : experimental molality of anion it can be determined directly from m_c and m_{c}' .

During calculation, the ternary Pitzer parameters change to minimize the objective function ω , by the Nelder-Mead method. So, the Pitzer parameters are now obtained by minimizing ω , and the resulting parameters are then considered acceptable for use in the Pitzer model.

Table 2. The binary Pitzer parameters for both binary systems Ni(NO₃)₂, and Al(NO₃)₃ (Jouaiti et al., 2018)

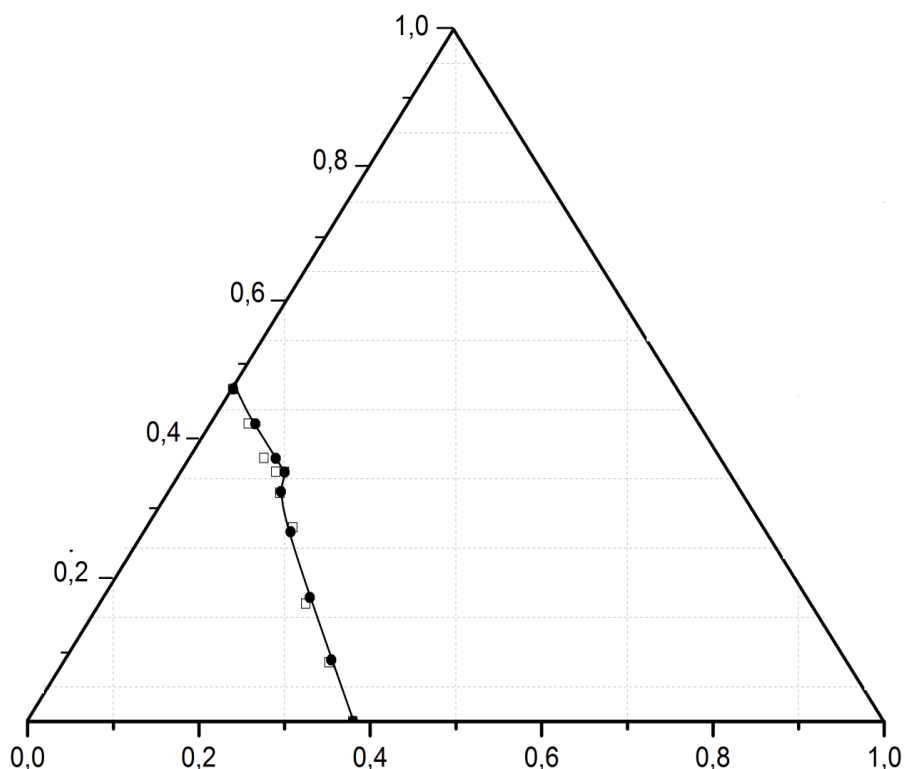
Salts	β^0	β^1	β^2	C^ϕ
Ni(NO ₃) ₂	0.288	1,437		-0,002
Al(NO ₃) ₃	0,703	1,890		0,075

Table 3. The ternary Pitzer parameters determining by iterative

Ternary parameters	$\theta_{Al,Ni}$	$\psi_{Al,Ni,NO3}$
Calculated	-0.267	-0.183

5. Comparison

Figure 2, shows the experimental isotherm for the studied ternary system in comparison with the theoretically elaborated one, using Pitzer model. As it's clear in the graph, the predicted solubilities agree very well with the experimental data.

**Fig. 2.** Experimental and calculated solubility of Al(NO₃)₃·9H₂O-Ni(NO₃)₂-H₂O system at 20°C, (□: experimental data,—●— calculated results obtained by using the Pitzer parameters in Table 2)

6. Conclusion

Because of the low solubility of Al(NO₃)₃·9H₂O, the Pitzer parameters cannot be determined from isopiestic measurements in the binary system. Therefore, solubilities in the ternary system

$\text{Al}(\text{NO}_3)_3\text{-Ni}(\text{NO}_3)_2\text{-H}_2\text{O}$ are applied to evaluate these parameters. Indeed, the successful calculations for the system proves that the obtained results experimentally are correct.

7. Conflict of interest

The authors declare that there is no conflict of interests regarding the publication of this paper. Also, they declare that this paper or part of it has not been published elsewhere.

References

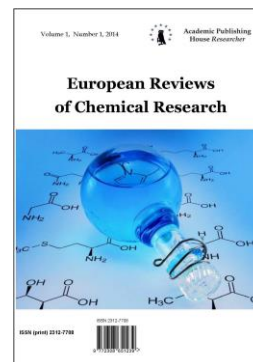
- Chretien et al., 2011 – Chretien A. (1992). Etude du système quaternaire. Eau, nitrate de sodium, chlorure de sodium, sulfate de sodium. *Ann. Chim*, 12: 26-54.
- Goundali et al., 2006 – El Goundali B., Kaddami M. (2006). Système ternaire : $\text{H}_2\text{O}\text{-Fe}(\text{NO}_3)_3\text{-Co}(\text{NO}_3)_2$ isotherme: 30 °C. *Comptes Rendus Chimie*, 9, 1488-1492.
- Jouaiti et al., 1983 – Barroug A., Laallam L., Boulghallat M., Jouaiti A. (1983). *Journal of Phase Equilibria and Diffusion*, 33(4): 310-314.
- Jouaiti et al., 2015 – Jouaiti A., Mekkaoui B., Boulghallat M., Barroug A., Lâallam L. (2015). Estimation of Pitzer Parameters for Aqueous salts equilibrium. Ternary system with a common ion. $\text{Al}(\text{NO}_3)_3\text{-Zn}(\text{NO}_3)_2\text{-H}_2\text{O}$. *International Journal of Applied Engineering Research*, 20: 41320-41322.
- Jouaiti et al., 2017 – Jouaiti M., Mekkaoui B., Lbibb R., Laallam L., Jouaiti A. (2017). Phase Diagram for the Ternary System $\text{Ni}(\text{NO}_3)_2\text{-Al}(\text{NO}_3)_3\text{-H}_2\text{O}$ between 20 and 40°C. *Der Pharma Chemica*, 9(18): 64-67.
- Jouaiti et al., 2018 – Mekkaoui B., Jouaiti M., Jouaiti A., Laallam L. (2018). Determination of Pitzer Parameters from Experimental Isotherm of a Ternary System Using Nelder Mead Method. *Der Pharma Chemica*, 10(2): 21-26.
- Kaddami et al., 1986 – Kaddami M. (1986). Thèse de doctorat, Lyon, no 57.
- Laallam et al., 2003 - Laallam L., Jouaiti A., El Allali S., M. Ferhat, Phase Diagram of the Ternary $\text{Cu}(\text{NO}_3)_2\text{-Zn}(\text{NO}_3)_2\text{-H}_2\text{O}$ System, *J. Mat. Lett.* 57(18), p 2707-2709.
- Laallam et al., 2004 – Laallam L., Kaddami M., El Allali S., Missali L., Tenu R., Berthet J., Counioux J.J. (2004). Diagramme de phases du système ternaire $\text{H}_2\text{O Al}(\text{NO}_3)_3\text{-Zn}(\text{NO}_3)_2$ entre 20 et 40 °C. *Ann. Chim. Mat.*, 29(4): 133-142.
- Laallam et al., 2011 – Laallam L., Jouaiti, A. Barroug A., El Allali S., Berthet J., Tenu R., Counioux J.J. (2011). Phase Diagram of the Quaternary $\text{Al}(\text{NO}_3)_3\text{-Cu}(\text{NO}_3)_2\text{-Zn}(\text{NO}_3)_2\text{-H}_2\text{O}$ System. *J. phase Equilib.*, 32(6): 543-550.
- Pitzer et al., 1974 – Pitzer K., Kim J.J. (1974). Thermodynamics of electrolytes, (3) Activity and osmotic coefficients for mixed electrolytes. *J. Am. Chem. Soc.*, 5701-5707.
- Pitzer et al., 1977 – Pitzer K. (1977). J. Phys. Thermodynamics of Electrolytes, (1) Theoretical basis and equations. *J. Phys. Chem.*, 268-277.
- Pitzer et al., 1977 – Pitzer K., Mayourga G. (1977). Thermodynamics of electrolytes, (2) Activity and osmotic coefficients for strong electrolytes with one or both ions univalent. *J. Phys. Chem.*, 77: 2300-2308.
- Schreinemakers et al., 1983 – Schreinemakers F.A.H. (1983). Graphical Deductions from the Solution Isotherms of A Double Salt and Its Components. *Z. Phys. Chem.*, 11: 109-765.
- Tenu et al., 1973 – Tenu R., Counioux J.-J., Cohen-Addad R. (1973). *Bull. Soc. Chim.*, Fr.82, 3.
- Tenu et al., 1979 – Tenu R., Counioux J.J. (1979). *Bull. Soc. Chim.*, 155: 5.

Copyright © 2019 by Academic Publishing House Researcher s.r.o.



Published in the Slovak Republic
European Reviews of Chemical Research
Has been issued since 2014.
E-ISSN: 2413-7243
2019, 6(1): 29-46

DOI: 10.13187/erchr.2019.1.29
www.ejournal14.com



Synthesis of Different Classes of Polyheterocyclic Cyanine Dyes: a Review

H.A. Shindy ^{a, *}

^a Department of Chemistry, Faculty of Science, Aswan University, Aswan 81528, Egypt

Abstract

In this review paper some synthesis of different classes of polyheterocyclic cyanine dyes have been reviewed. In this paper review detailed synthesis steps for the synthesis of some polyheterocyclic cyanine dyes were represented via equations. This is covers the synthesis of polyheterocyclic monomethine cyanine dyes (simple cyanine dyes), dimethine cyanine dyes, trimethine cyanine dyes (carbocyanine dyes), pentamethine cyanine dyes (dicarbocyanine dyes), styryl cyanine dyes (hemicyanine dyes), aza-styryl cyanine dyes (aza-hemicyanine dyes) and apocyanine dyes. Besides, in the introduction section of this review paper some light is focused on some important uses, applications, characterizations and properties of cyanine dyes. This review paper is very readable, informative, and useful for synthetic dye chemists, researchers and students who look for the different methods in the synthesis and preparation of various classes of polyheterocyclic cyanine dyes. In addition, this paper review can be used and/or will be most valuable as a thesis and/or as a note book for student lectures, particularly for the post graduate students and researchers in the field of heterocyclic and/or cyanine dyes chemistry. This special and/or specific type of collective review in the synthesis of different classes of only polyheterocyclic cyanine dyes has been paid no attention and is absence in the chemistry literature.

Keywords: cyanine dyes, synthesis, polyheterocyclic cyanine dyes, different classes of cyanine dyes, uses of cyanine dyes, applications of cyanine dyes, properties of cyanine dyes.

1. Introduction

The first cyanine dye was discovered in 1856 by C.H. Greville Williams. Later in 1873, H.W. Vogel began to use cyanine dyes in photography (Hamer, 1964). Since then, research on cyanine dyes developed (Chen, 2006) rapidly due to their extra sensitizing power on silver halide in the region of spectra from visible to near infrared (IR) in photography.

Cyanine dyes (Shindy, 2014; Shindy, 2015; Shindy 2015a; Shindy 2012) have relatively good stability, high molar absorption coefficients, medium fluorescence intensity, narrow spectrum width and the ability to form H- or J-aggregates. The maximum absorption wavelength of cyanine dyes can be tuned precisely from near-UV to near-IR by chemical structure modification. With these unique photophysical and photochemical properties, cyanine dyes are recently being used in many applications such as nonlinear optics, optical data storage, bimolecular labeling, dye laser, photorefractive materials and photodynamic therapy (Mishra et al., 2000).

In recent years, there has been increased interest in the field of the synthesis and application of cyanine dyes absorbing in different visible spectral regions, suitable as nucleic acid labels.

* Corresponding author
E-mail addresses: hashindy2@hotmail.com (H.A. Shindy)

The number of both patents (Roth et al., 1995; Yue et al., 1996; Yue et al., 1994; Yue et al., 1997; Lee, 1997) and scientific publications (Deligeorgiev et al., 1995; Deligeorgiev et al., 1998; Yarmoluk, et al., 1996; Moreda et al., 1997) is an strong evidence for the commercial (Haugland, 1996), scientific (Timcheva et al., 1997; Zeng et al., 1997; Josef et al., 1996; Millard et al., 1997; Roth et al., 1997; Gurrieri et al., 1997; Clark et al., 1997) and practical importance of these probes in nucleic acid research, clinical and environmental analysis.

Additional important and interesting properties, characterizations and applications of cyanine dyes ((Shindy, 2016; Shindy, 2017; Shindy, 2018; Shindy, 2018a; Shindy et al., 2018) also covers and/or includes the following:

1-Cyanine dyes are photosensitizers dyes, and this can be evaluated through examining their electronic visible absorption spectra in 95 % ethanol solution. The cyanine dyes were thought to be better photosensitizers when they absorb the visible light to initiate the electronic transitions at higher wavelength bands (bathochromic shifted and/or red shifted dyes). Consequently, the photosensitization of the cyanine dyes decreases when they absorb the visible light to initiate the electronic transitions at lower wavelength bands (hypsochromic shifted and/or blue shifted dyes). So, we may say that the photosensitization of one cyanine dye is higher than the other one if the wavelength of the maximum absorption spectrum of the former one is longer than that of the latter one. In contrary, we may say that the photosensitization of one cyanine dye is lower than the other one if the wavelength of the maximum absorption spectrum of the former one is shorter than that of the latter one. Studying the electronic visible spectra of cyanine dyes in 95 % ethanol solution is very important in the case of cyanine dyes because the extensive uses of these dyes as photographic sensitizers for silver halide emulsion in photosensitive material industry for colored and non colored (black and white) films (cyanine dyes were originally used, and still are, to increase the sensitivity range of photographic emulsions, i. e. to increase the range of wavelengths which will form an image on the film).

2-Cyanine dyes are solvatochromic dyes, and this can be evaluated through measuring their electronic visible absorption spectra in pure solvent having different polarities The cyanine dyes were thought to be better solvatochromic properties when they give strong positive and/or negative solvatochromism in pure solvents having different polarities. Consequently, the solvatochromic properties of the cyanine dyes decrease when they give weak positive and/or negative solvatochromism in pure solvent having different polarities. So, we may say that the solvatochromic properties of one cyanine dye is higher than the other one if the positive and/or the negative solvatochromism in pure solvents having different polarities of the former one is stronger than that of the latter one. In contrary we may say that the solvatochromic properties of one cyanine dye is lower than the other one if the positive and/or the negative solvtochromism in pure solvnt having different polarities of the former one is weaker than that of the latter one. Positive solvatochromism reveals bathochromic shifted (red shifted) absorption bands with increasing solvent polarity. In contrast, negative solvatochromism discloses hypsochromic shifted (blue shifted) bands with increasing solvent polarity. Solvatochromic evaluation study is very important in the case of cyanine dyes because the extensive uses and application of these dyes in textile industry and/or as probes for determining solvent polarity in physical, physical organic, inorganic and/or solution chemistry.

3-Cyanine dyes are halochromic dyes, and this can be evaluated through examining their electronic visible absorption spectra in aqueous universal buffer solutions owing varied pH values. The cyanine dyes were thought to be better halochromic properties when they give strong positive and/or negative halochromism in aqueous universal buffer solutions having varied pH values. Consequently, the halochromic properties of the cyanine dyes decrease when they give weak positive and/or negative halochromism in aqueous universal buffer solutions having varied pH values. So, we may say that the halochromic properties of one cyanine dye is higher than the other one if the positive and/or the negative halochromism of the former one in aqueous universal buffer solutions having varied pH values is stronger than that of the latter one. In contrary we may say that the halochromic properties of one cyanine dye is lower than the other one if the positive and/or the negative halochromism of the former one in aqueous universal buffer solutions having varied pH values is weaker than that of the latter one. Positive halochromism means occurrence of a bathochromic shifted (red shifted) absorption bands with changing solution pH of the buffer solution. In contrast, negative halochromism means occurrence of a hypsochromic shifted (blue

shifted) absorption bands with changing the pH of the buffer solution. Halochromic evaluation study in aqueous universal buffer solutions having varied pH values have a great practical importance in the case of cyanine dyes because the wide uses and applications of these dyes as indicators in operations of acid / base titrations in analytical chemistry.

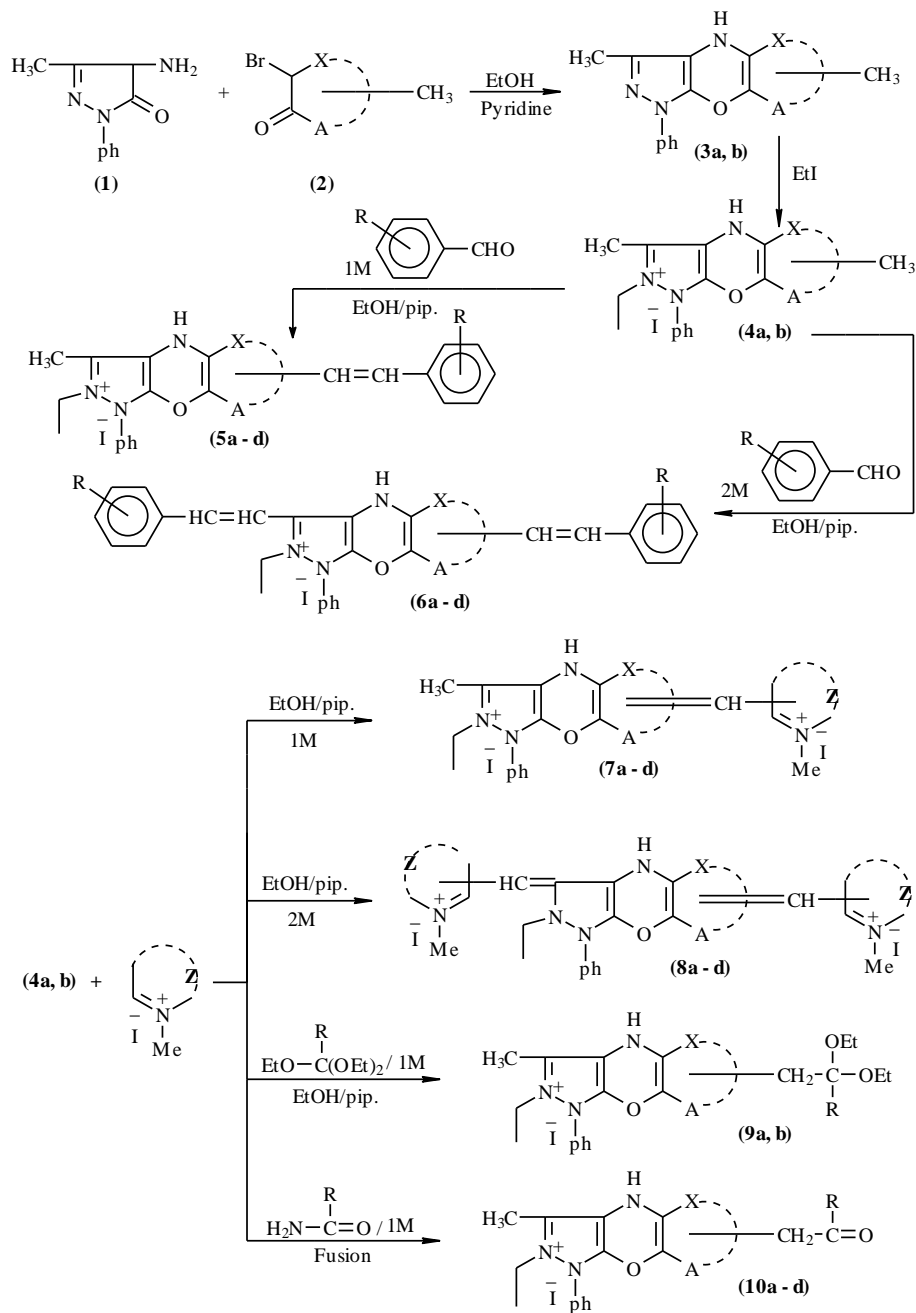
4-Cyanine dyes are biologically (antimicrobial) active dyes, and this can be evaluated through measuring their inhibition zone diameter against a number of bacterial and/or fungi strains. The cyanine dyes were thought to be better antimicrobial active when they give higher inhibition zone diameter against the tested bacterial and/or the fungi strains. Consequently, the antimicrobial activity of the cyanine dyes decrease when they give lower inhibition zone diameter against the tested bacterial and/or the fungi strains. So, we may say that the antimicrobial activity of one cyanine dye is stronger than the other one if the inhibition zone diameter against the tested bacterial and/or the fungi strains of the former one is higher than that of the latter one. In contrary, we may say that the antimicrobial activity of one cyanine dye is weaker than the other one if the inhibition zone diameter against the tested bacterial and/or the fungi strains of the former one is lower than that of the latter one. Studying the antimicrobial activity evaluation against a number of bacterial and/or fungi strains bears to have a great practical value in the case of cyanine dyes because the extensive uses and applications of these dyes as bactericidal (anti-bacterial strains) and/or as fungicidal (anti-fungi strains) in pharmaceutical (pharmacological) industry and/or in pharmacology.

5-Cyanine dyes are rich electronic transitions dyes, and this can be evaluated through investigating their electronic visible absorption spectra in 95 % ethanol solution. The dyes were thought to be better electronic transitions when they absorb light at higher wavelength bands (bathochromic shifted and/or red shifted dyes). Consequently, the electronic transitions of the dyes decreases when they absorb light at lower wavelength bands (hypsochromic shifted and/or blue shifted dyes). So, we may say that the electronic transitions of one cyanine dye is higher than the other one if the wavelength of the maximum absorption spectrum of the former one is longer than that of the latter one. In contrary, we may say that the electronic transitions of one cyanine dye is lower than the other one if the wavelength of the maximum absorption spectrum of the former one is shorter than that of the latter one. Studying the visible electronic transition absorption spectra in 95 % ethanol solution is very important in the case of cyanine dyes because the wide uses and applications of these dyes as photographic sensitizers in photographic material industry.

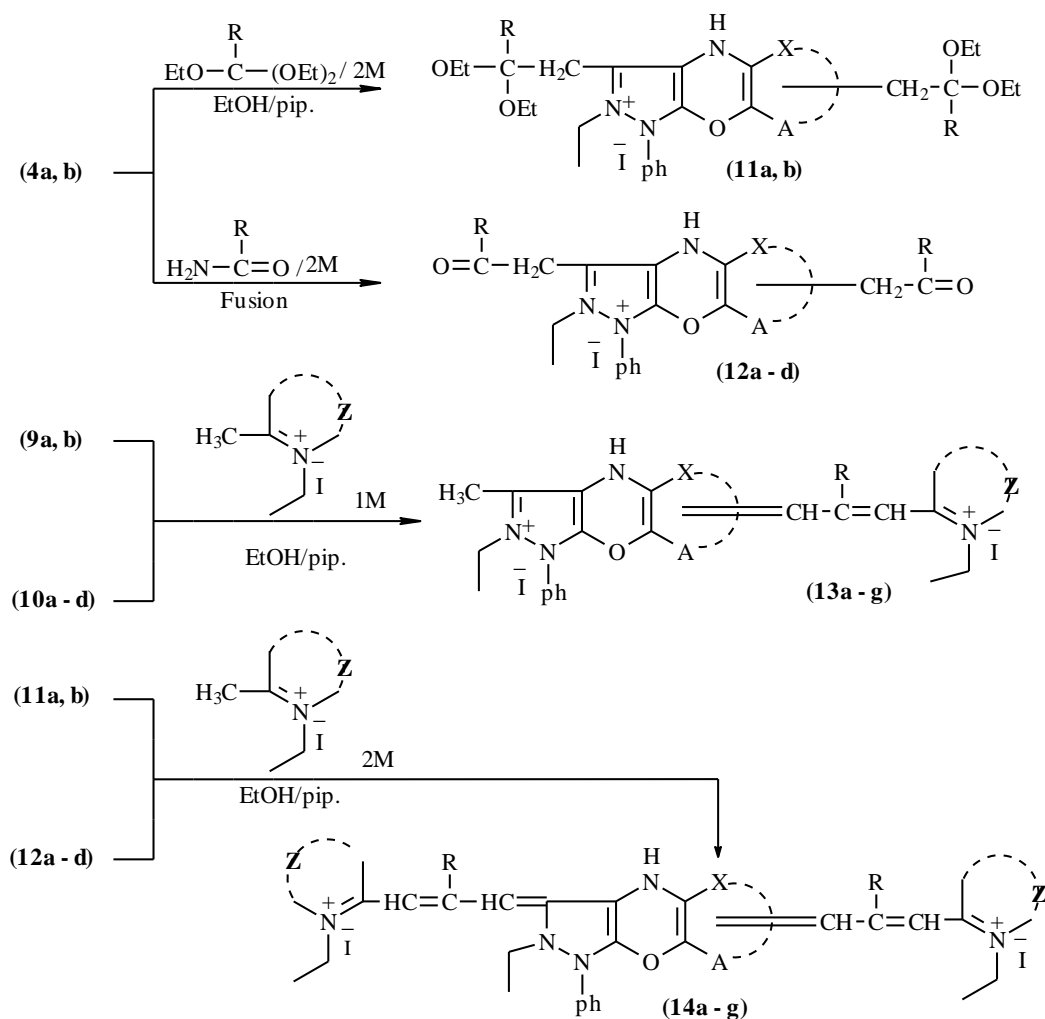
6-Cyanine dyes are anti-tumor and/or anti-cancer dyes, and this can be explained in the light of their extensive uses and applications in photodynamic therapy (PDT). Photodynamic therapy (PDT) is a new technique and/or method for treatment of cancer. Due to their excellent properties, cyanine dyes are used in light power treatment. Photodynamic therapy has many advantages compared with surgery chemotherapy and radiotherapy treatment in treating cancer. First of all, it can have special light sensitive materials accumulate in tumor selectively, which will not damage the body normal tissues cells. Secondly, only local anesthetic is needed which saves a lot of medical bills. Finally, the side effect is small, which does not cause other damage in the body. Because of its light selectivity and specificity, photodynamic therapy only damage tumor tissue without harming the body normal cells. Particularly, merocyanine dyes can distinguish some certain cells and selectively enter into cancer cells, then kill it as photosensitizers directly using for photodynamic therapy (PDT) or as radiation sensitizers for the treatment of solid tumors, where the affinity between cyanine dyes and tumor cells is much higher than that between cyanine dyes and normal cells. Merocyanine dyes are also used as antitumor drugs and combining PDT with drug therapy has become a tendency and will certainly promote the treatment of tumors.

2. Synthesis of Different Classes of Polyheterocyclic Cyanine Dyes

Styryl cyanines (5a-d), (6a-d), monomethine cyanine dyes (7a-d), (8a-d) and trimethine cyanine dyes (13a-g), (14a-g) incorporating bis pyrazolo-[2,3-b; 2',3'-b'] oxazine and/or pyrazolo [2,3-b]-oxazolo[2',3'-b']oxazine were prepared (Osman et al., 1997), Scheme (1).



Scheme (1)



Scheme (1) continue

Substituents in Scheme (1):

(3a, b): X(A)= 3[1-phenyl pyrazole] (a); X(A)= 6[oxazole] (b).

(4a, b): X(A)= 3[1-phenyl pyrazolium-2-yl salt] (a);

X(A)= 6[oxazolium-5-yl salt] (b).

(5a-d); (6a-d): X(A)= 3[1-phenyl pyrazolium-2-yl salt]; R= H(a), ρ .OCH₃ (b), ρ .NO₂ (c);

X(A)= 6[oxazolium-5-yl salt]; R= ρ .OCH₃ (d).

(7a-d);(8a-d): X(A)=3[N-ethyl pyrazole], Z= 1-methyl pyridinium-4-yl salt (a);

X(A)= 3[N-ethyl pyrazole], Z= 1-methyl quinolinium-4-yl salt (b);

X(A)= 3[N-ethyl pyrazole], Z= 2-methyl isoquinolinium-1-yl salt (c);

X(A)= 6[N-ethyl oxazole], Z= 1-methyl quinolinium-4-yl salt (d).

(9a, b); (11a, b): X(A)= 3[1-phenyl pyrazolium-2-yl salt], R= H (a);

X(A)= 6[oxazolium-5-yl salt], R= H (b).

(10a-d); (12a-d): X(A)= 3[1-phenyl pyrazolium-2-yl salt]; R= CH₃ (a),

CF₃ (b), C₆H₅ (c). X(A)= 6[oxazolium-5-yl salt], R= CH₃ (d).

(13a-g); (14a-g): X(A)= 3[N-ethyl pyrazole], R= H, Z= 1-ethyl pyridinium-2-yl salt (a);

X(A)= 3[N-ethyl pyrazole], R= H, Z= 1-ethyl quinolinium-2-yl salt (b);

X(A)= 6[N-ethyl oxazole], R= H, Z= 1-ethyl quinolinium-2-yl salt (c);

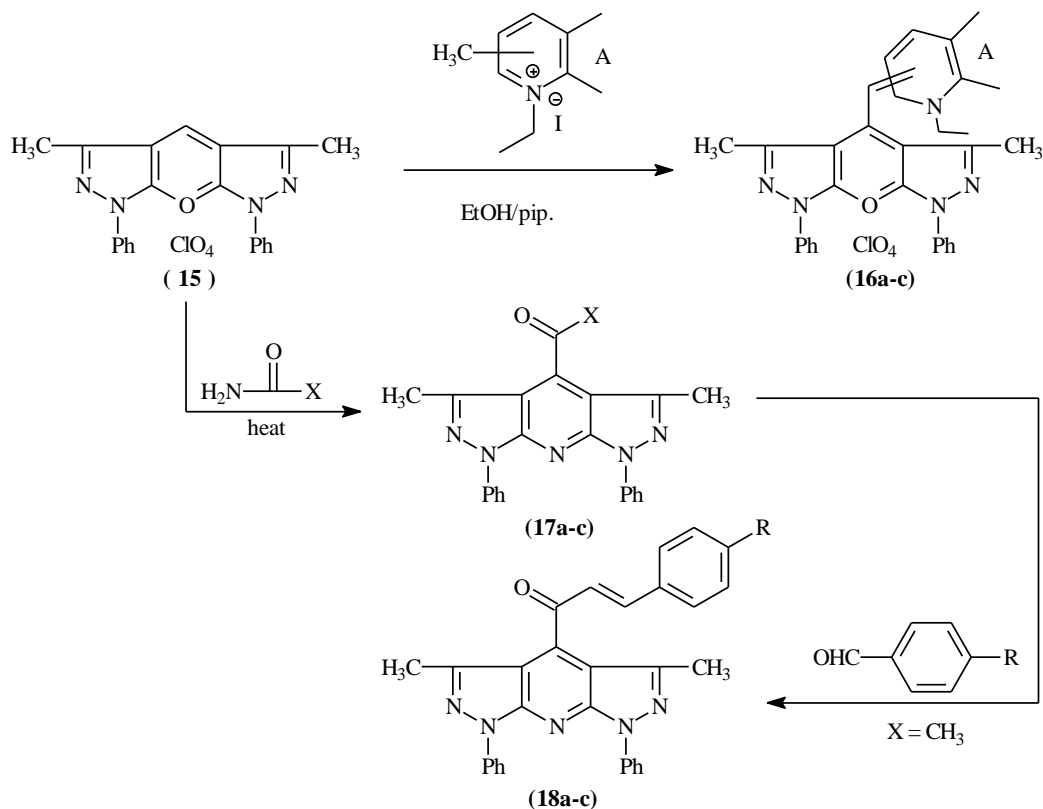
X(A)= 3[N-ethyl pyrazole], R= CH₃, Z= 1-ethyl quinolinium-2-yl salt (d);

X(A)= 3[N-ethyl pyrazole], R= CF₃, Z= 1-ethyl quinolinium-2-yl salt (e);

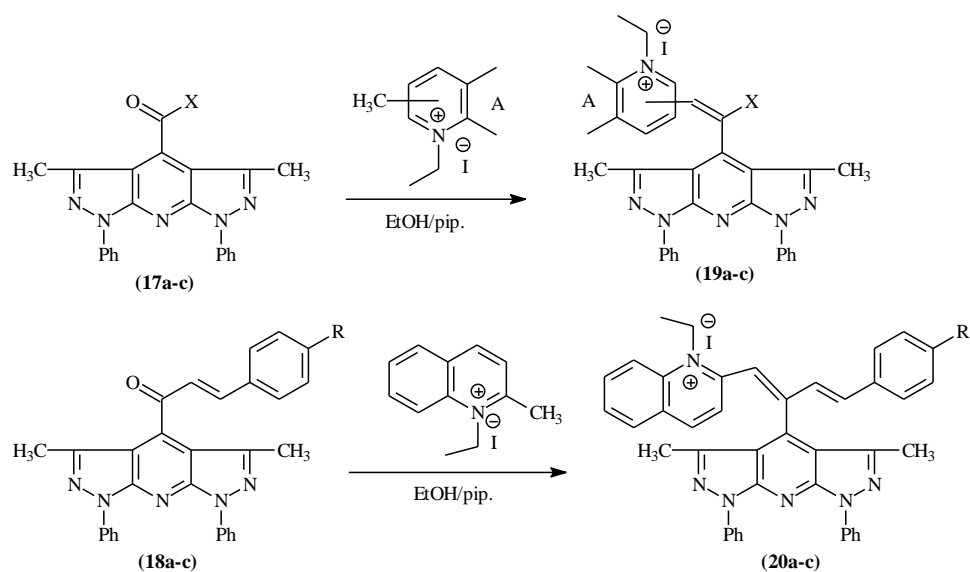
X(A)= 3[N-ethyl pyrazole], R= C₆H₅, Z= 1-ethyl quinolinium-2-yl salt (f);

$X(A) = 6[N\text{-ethyl oxazole}], R = \text{CH}_3, Z = 1\text{-ethyl quinolinium-2-yl salt (g)}$.

Monomethine, β -substituted dimethine and styryl cyanine dyes were synthesized using oxonium salts (El-Aal, et al., 2005), Scheme (2).



Scheme (2)



Scheme (2) continue

Substituents in Scheme (2):

(16a-c): A = 1-ethylpyridine-2-ium (a); 1-ethylquinoline-2-ium (b);
1-ethylpyridine-4-ium (c).

(17a-c): X = H (a); CH₃ (b); ph (c).

(18a-c): R = H (a); OH (b); NO₂ (c).

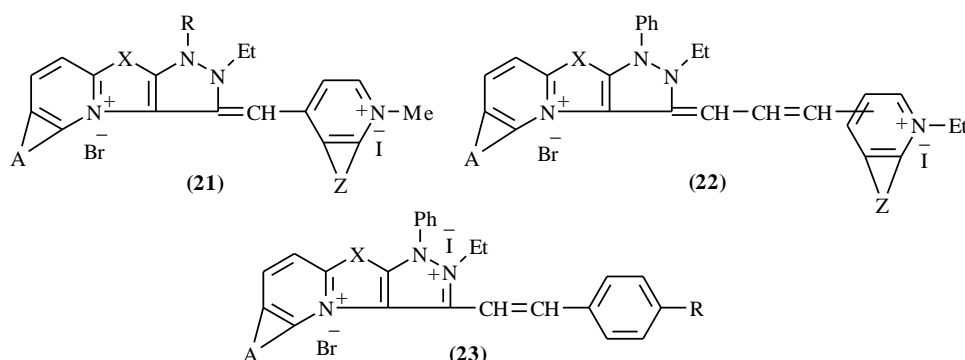
(19a-c): X = H, A = 1-ethylquinoline-2-ium (a);

X = CH₃, A = 1-ethylquinoline-2-ium (b);

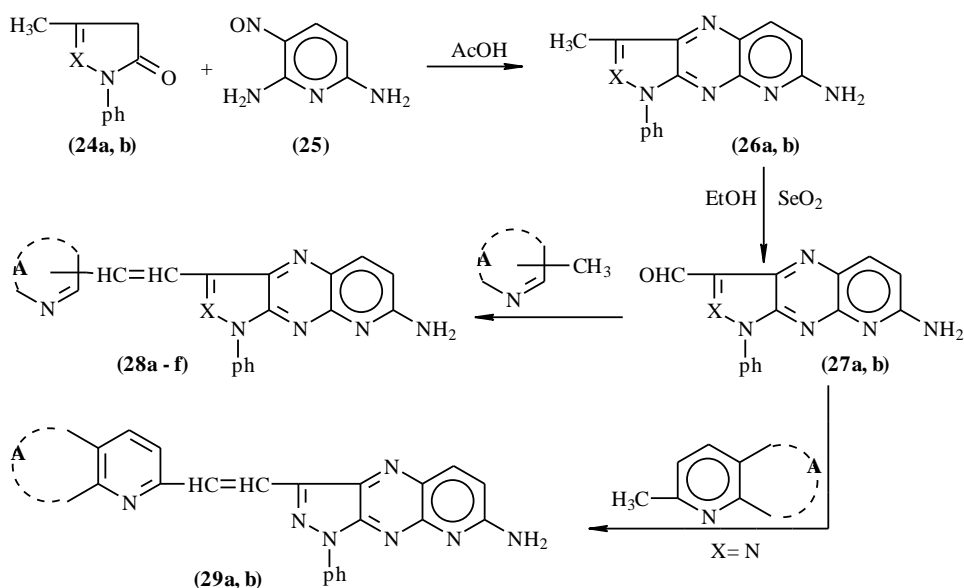
X = ph, A = 1-ethylquinoline-2-ium (c).

(20a-c): R = H (a); OH (b); NO₂ (c).

Monomethine cyanines (21, R = H, ph; X = NH, CH₂; A = H, C₄H₄; Z = H, C₄H₄), trimethine cyanines (22, X = NH, CH₂; A = H, C₄H₄; Z = H, C₄H₄) and styryl cyanines (23, R = H, OMe, NO₂; X = NH, CH₂; A = H, C₄H₄) were synthesized (Abu El-Hamd, 1996), Scheme (3).

**Scheme (3)**

Dimethine cyanines (28a-f) and their bases (29a, b), incorporating pyrazolo (3,4-d)-8-amino-1-azaquinoxaline moiety or its ethiodide, have been prepared (El-Maghraby, et al., 1988), Scheme (4).

**Scheme (4)**

Substituents in Scheme (4):(24, 26, 27): X= N(a); N⁺ – EtI⁻ (b).

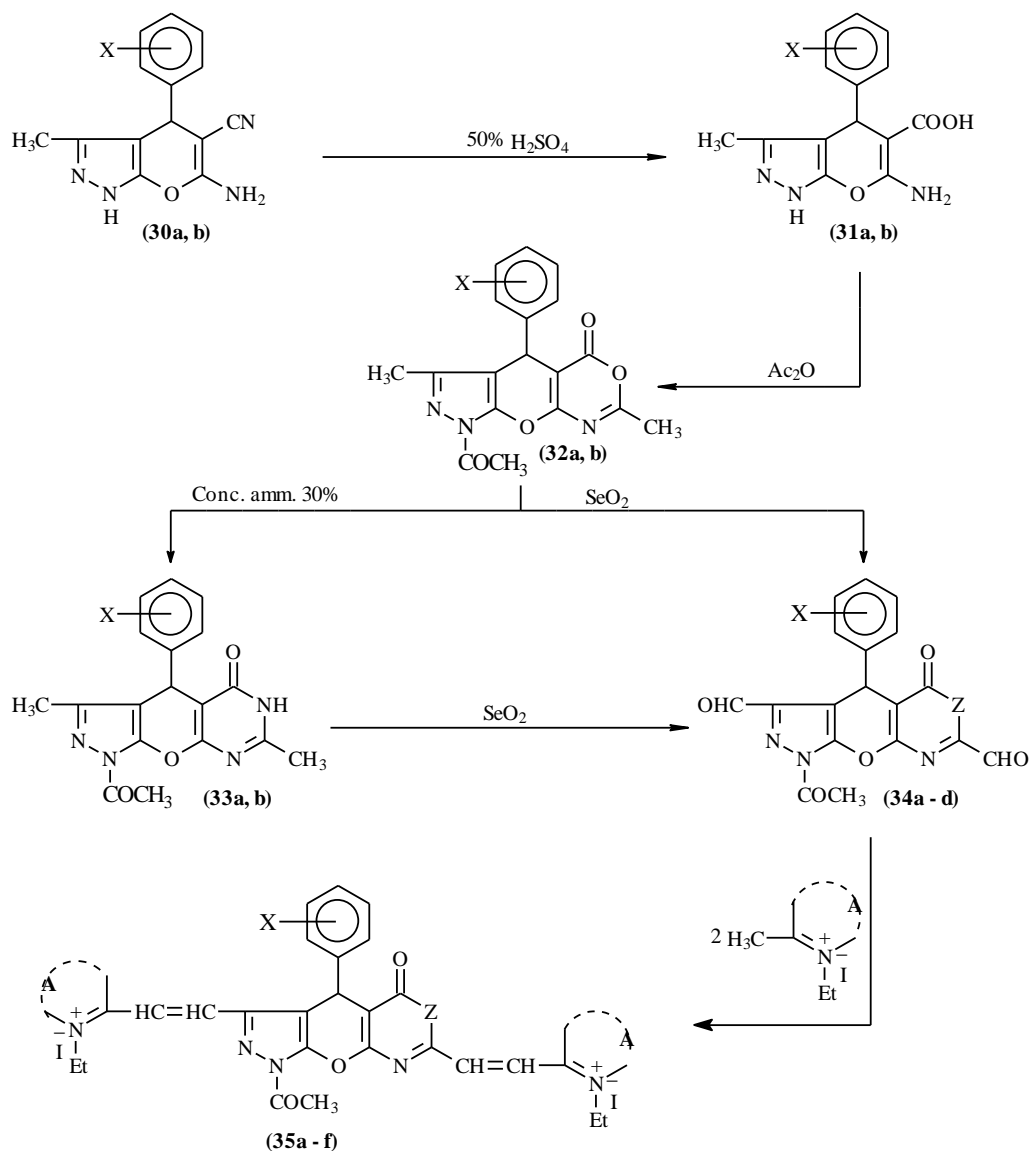
(28a-f): X= N, A= 1-ethyl pyridinium-2-yl salt (a);

X= N, A= 1-ethyl quinolinium-2-yl salt (b);

X= N, A= 1-ethyl pyridinium-4-yl salt (c);

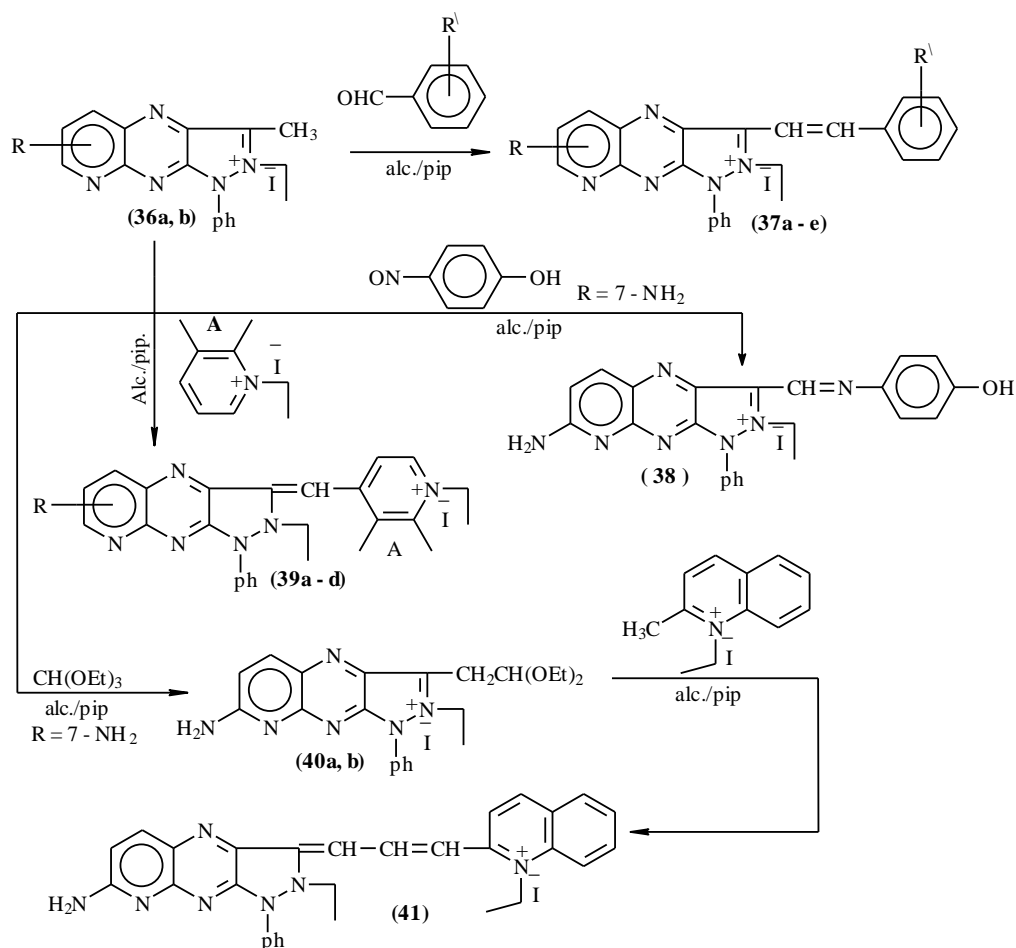
X= N⁺-EtI⁻, A= 1-ethyl pyridinium-2-yl salt (d);X= N⁺-EtI⁻, A= 1-ethyl quinolinium-2-yl salt (e);X= N⁺-EtI⁻, A= 1-ethyl pyridinium-4-yl salt (f).(29a, b): A= H(a); C₄H₄ (b).

Dicationic cyanine dyes containing pyrazolo pyrano-oxazone/ pyrimidine moiety have been prepared and their visible absorption spectra have been studied (El-Maghraby et al., 1991), Scheme (5).

**Scheme (5)****Substituents in Scheme (5):**(30a, b), (31a, b), (32a, b), (33a, b): X = *p*.Cl (a), *p*.NO₂ (b).(34a – d): X = *p*.Cl, Z = O (a); X = *p*.Cl, Z = NH (b);X = *p*.NO₂, Z = O (c); X = *p*.NO₂, Z = NH (d).(35a – f): X = *p*.Cl, Z = O, A = 1-ethyl pyridinium-2-yl salt (a);X = *p*.Cl, Z = NH, A = 1-ethyl pyridinium-2-yl salt (b);

- X = ρ .Cl, Z = O, A = 1-ethyl quinolinium-2-yl salt (c);
 X = ρ .Cl, Z = NH, A = 1-ethyl quinolinium-2-yl salt (d);
 X = ρ .NO₂, Z = O, A = 1-ethyl quinolinium-2-yl salt (e);
 X = ρ .NO₂, Z = NH, A = 1-ethyl quinolinium-2-yl salt (f).

A series of pyrazolo[4,5-b] pyrido[2,3-c] pyrazine cyanine dyes covering styryl, aza-styryl, mono- and tri- methine cyanines were synthesized via reaction of 3-methyl-1-phenyl pyrazolo [4,5-b] pyrido [2,3-c] pyrazine-2-ethyl iodide with active components (Khalafalla et al., 1993), Scheme (6).

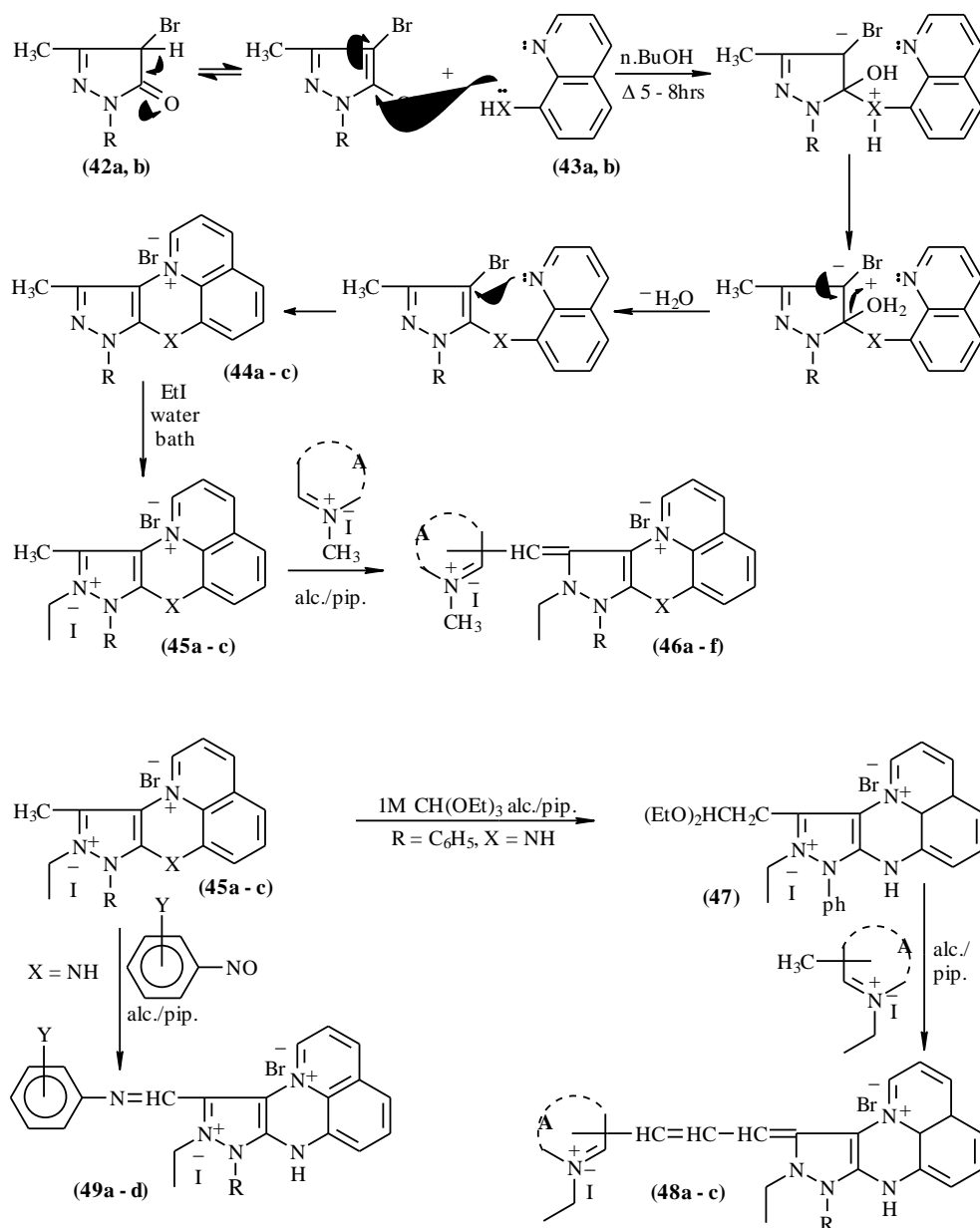


Scheme (6)

Substituents in Scheme (6):

- (36a, b): R = 6-Br (a); 7-NH₂ (b).
 (37a – e): R = 6-Br, R' = H (a), ρ .N(CH₃)₂ (b), ρ .NO₂ (c),
 R = 7-NH₂, R' = H (d), ρ .OH (e).
 (39a – d): R = 7-NH₂, A = 1-ethyl pyridinium-4-yl salt (a),
 R = 7-NH₂, A = 1-ethyl quinolinium-4-yl salt (b),
 R = 7-NH₂, A = 2-ethyl isoquinolinium-1-yl salt (c),
 R = 6-Br, A = 2-ethyl isoquinolinium-1-yl salt (d).

A number of mono-(tri-)methine and aza-methine cyanine dyes of pyrazolo [5,4-b] quinolino[a,b]-1,4-pyra-(oxa)-zinium bromide salts were prepared (Koraïem et al., 1999), Scheme (7).



Scheme (7)

Substituents in Scheme (7):

 (42a, b): R = H (a); C₆H₅ (b).

(43a, b): X = NH (a); O (b).

 (44a - c); (98a - c): R = C₆H₅, X = NH (a);

 R = C₆H₅, X = O (b); R = H, X = NH (c).

 (46a - f): R = C₆H₅, X = NH, A = 1-methyl pyridinium-4-yl salt (a);

R = H, X = NH, A = 1-methyl pyridinium-4-yl salt (b);

 R = C₆H₅, X = NH, A = 1-methyl quinolinium-4-yl salt (c);

 R = C₆H₅, X = O, A = 1-methyl quinolinium-4-yl salt (d);

 R = C₆H₅, X = NH, A = 2-methyl isoquinolinium-1-yl salt (e);

 R = C₆H₅, X = O, A = 2-methyl isoquinolinium-1-yl salt (f).

(48a - c): A = 1-ethyl pyridinium-2-yl salt (a);

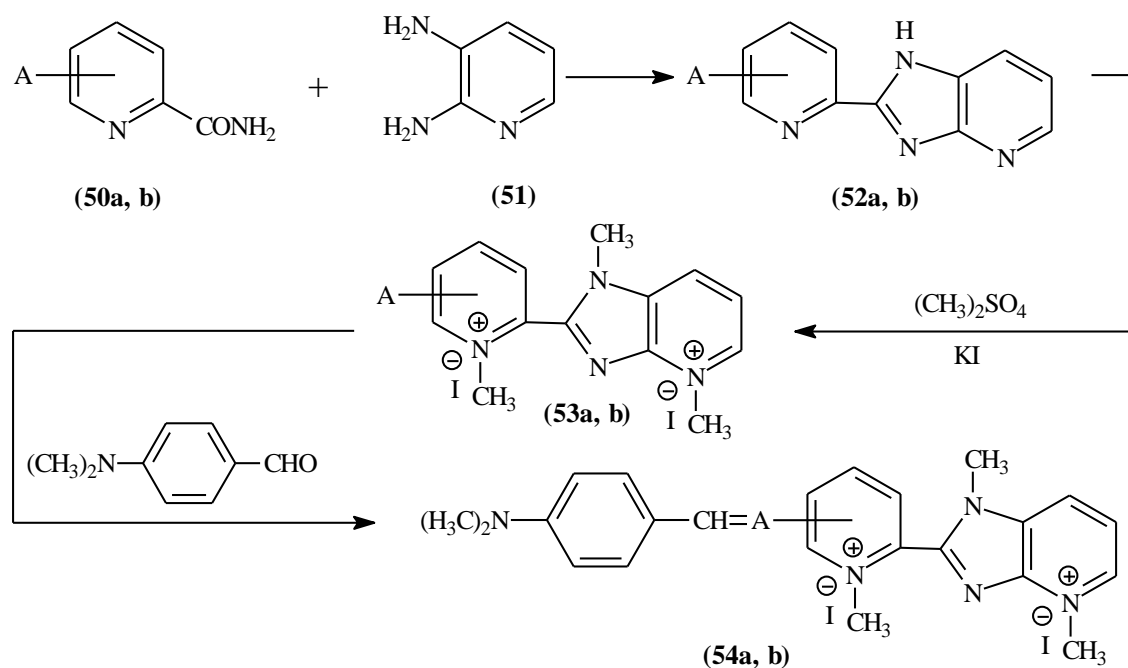
A = 1-ethyl quinolinium-2-yl salt (b);

A = 1-ethyl pyridinium-4-yl salt (c).

 (49a - d): R = C₆H₅, Y = 4.OH (a); R = H, Y = 4.OH (b);

R = C₆H₅, Y = 2.OH, 5,6-benzosubstituent (c);
 R = C₆H₅, Y = 2.OH, 3,4-benzosubstituent (d).

Savarino, et al., synthesized new styryl cyanine dyes by quaternization of 2[2(4)-methyl pyridyl]-imidazo[4,5-b]pyridine and further reaction with p.dimethylamino-benzaldehyde (Savarino et al., 1987), Scheme (8).



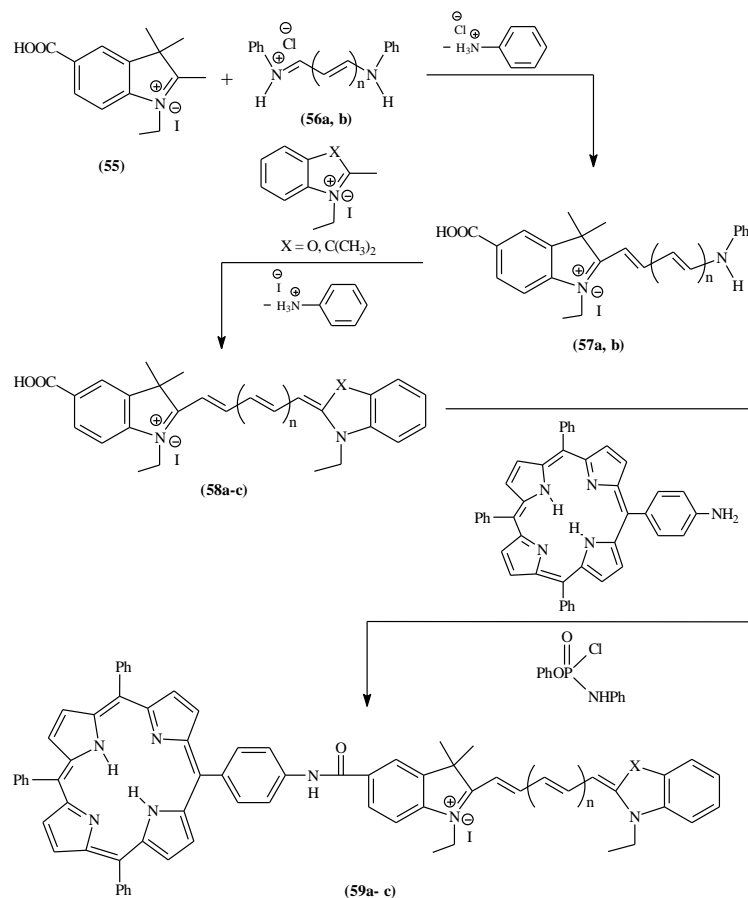
Scheme (8)

Substituents in Scheme (8):

(50a, b); (52a, b); (53a,b): A = 2-methyl (a); 4-methyl (b).

(54a, b): A = 2-methine (a); 4-methine (b).

Lindsey, et al., prepared three members of a new class of photochemical model compounds containing a covalently-linked porphyrin and a cyanine dye (Lindsey et al., 1989), Scheme (9).



Scheme (9)

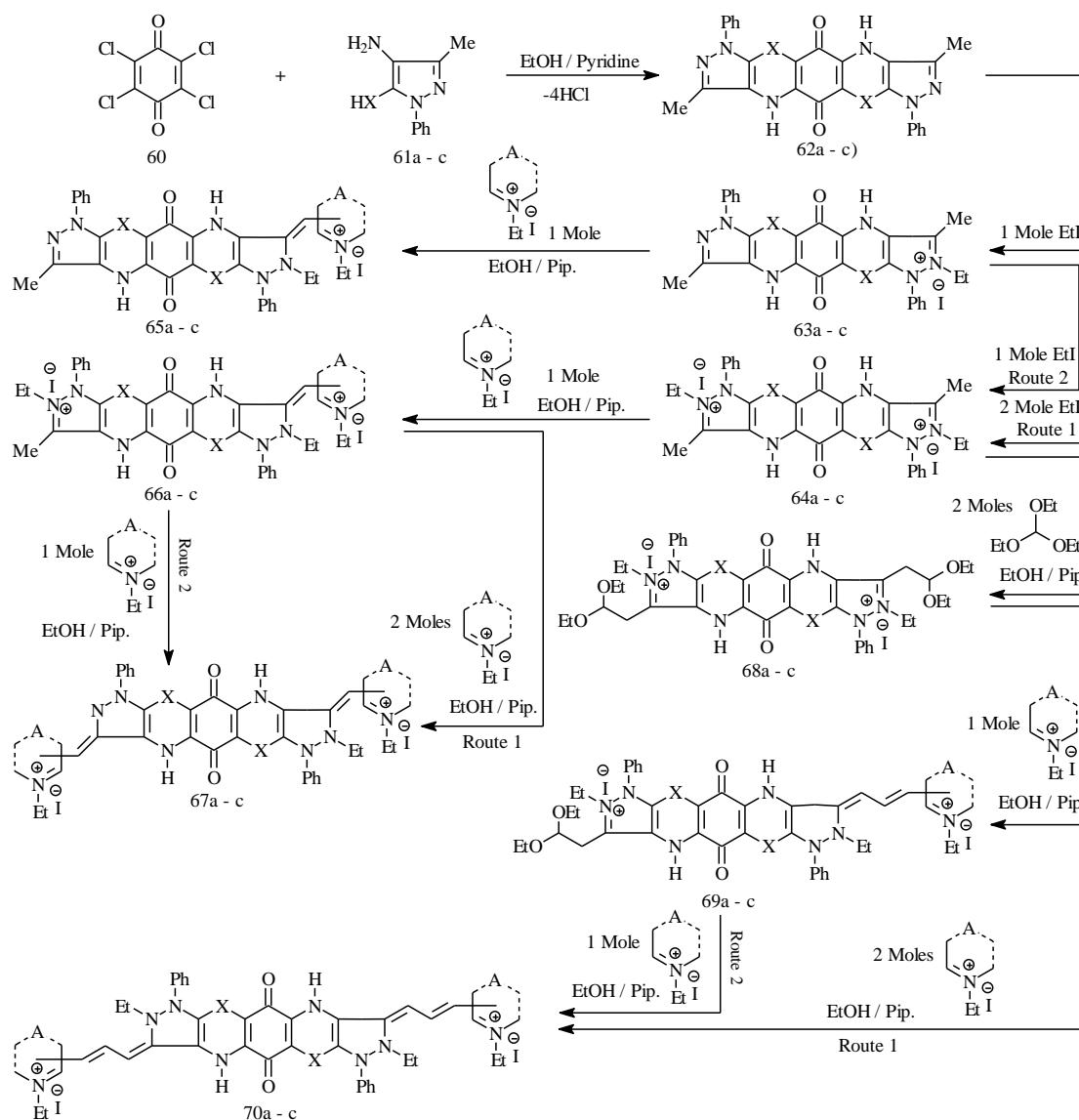
Substituents in Scheme (9):

(56a, b); (57a, b): $n = 0$ (a); 2 (b).

(58a - c); (59a - c): X = O, $n = 0$ (a); X = C(CH₃)₂, $n = 0$ (b);

X = C(CH₃)₂, $n = 2$ (c).

Shindy, et al. prepared a series of cyanine dyes including monomethine cyanine dyes (simple cyanine dye) and trimethine cyanine dyes (carbocyanine dyes) incorporating benzo[2,3-b, 2',3'-b']bispyrazolo[4,5-b]-1,4-(oxa-, thia- and pyra-)zine-6,12-dione (Shindy et al., 2006), Scheme (10).



Scheme (10)

Substituents in Scheme (10):

(61a-c); (62a-c); (63a-c); (64a-c) & (68a-c): X = O (a); X = S (b); X = NH (c).

(65a-e); (66a-e) & (67a-e): X = O, A = 1-ethyl pyridinium-4-yl salt (a);

X = O, A = 1-ethyl quinolinium-4-yl salt (b);

X = O, A = 2-ethyl isoquinolinium-1-yl salt (c);

X = S, A = 1-ethyl quinolinium-4-yl salt (d);

X = NH, A = 1-ethyl quinolinium-4-yl salt (e).

(69a-g) & (70a-g): X = O, A = 1-ethyl pyridinium-2-yl salt (a);

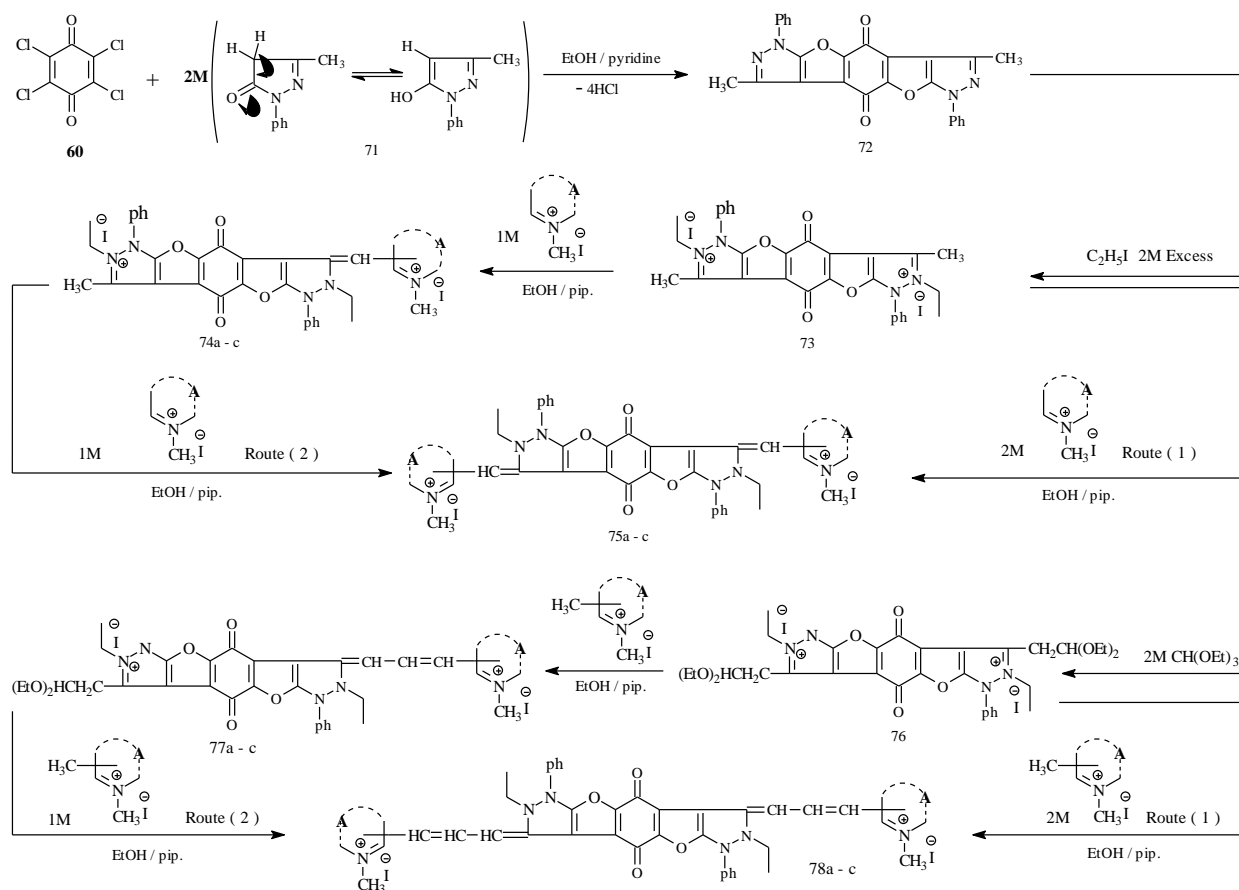
X = O, A = 1-ethyl quinolinium-2-yl salt (b);

X = O, A = 1-ethyl pyridinium-4-yl salt (c);

X = S, A = 1-ethyl quinolinium-2-yl salt (d);

X = NH, A = 1-ethyl quinolinium-2-yl salt (e).

Shindy synthesized a number of monomethine cyanine dyes, bis monomethine cyanine dyes, trimethine cyanine dyes and bis trimethine cyanine dyes having benzo[2,3-b; 2',3'-b']bis furo[3,2-d]pyrazole nuclei (Shindy, 2007), Scheme (11).



Scheme (11)

Substituents in Scheme (11):

(74a-c); (75a-c): A = 1-methyl pyridinium-4-yl salt (a);

A = 1-methyl quinolinium-4-yl salt (b);

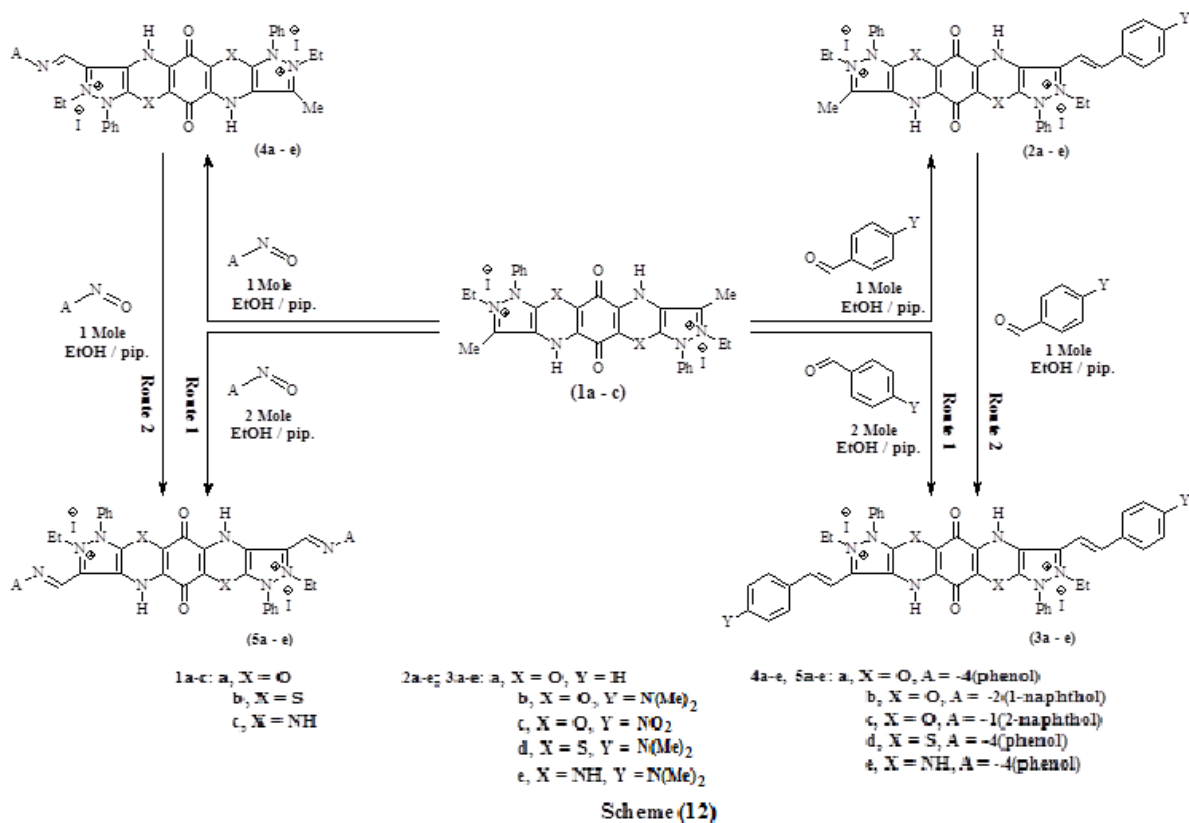
A = 2-methyl isoquinolinium-1-yl salt (c).

(77a-c); (78a-c): A = 1-methyl pyridinium-2-yl salt (a);

A = 1-methyl quinolinium-2-yl salt (b);

A = 1-methyl pyridinium-4-yl salt (c).

Hemicyanine dyes and aza-hemicyanine dyes derived from benzo[2,3-b; 2',3'-b']bis pyrazolo[4,5-b]-1,4-(oxa-, thia-, and pyra)-zine-6,12-dione ring system were prepared by Shindy et al. (Shindy et al., 2014), Scheme (12).

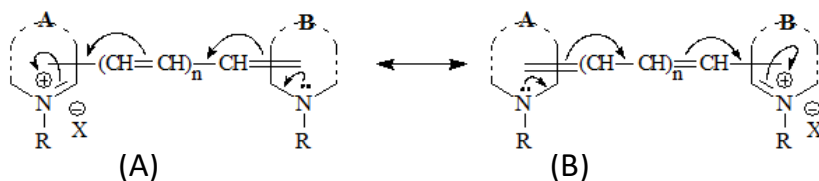


Scheme (12)

3. Conclusion

1. Cyanine dyes are comprised of two heterocycles containing nitrogen linked together by a conjugated polymethine chain. The heterocycles act as both electron donors and acceptors creating an push-pull system throughout the molecule, allowing for long wavelength absorption, Scheme (13).

2. The intensity of the colour of the cyanine dyes is illustrated according to suggested two mesomeric electronic transitions structures (two resonance forms) (A) and (B) producing a delocalized positive charges over the conjugated chromophoric group system of the dyes, Scheme (13).



(n = 0, 1, 2, 3; etc.); R=CH₃, CH₃CH₂;

X=I; A=Heterocyclic nucleus; B=Heterocyclic nucleus

**Structure and colour intensity illustration of cyanine dyes
Scheme (13)**

3. Modification of cyanine dyes structures can be carried out through the following:

a-The use of heterocycles with different hetero atoms.

b-The use of heterocycles with different substituents on the carbon skeleton.

c-The use of heterocycles with different substituents on the nitrogen atom of the heterocycles.

d-The use of heterocyclic with different ring size system (five membered ring, six membered ring, etc.)

e-The use of heterocyclic with different nuclear number (mono nuclear, bi nuclear and/or polynuclear).

f-The change and/or replacing the substituents in the meso substituted side chain of the polymethine bridge.

g-Increasing and/or decreasing conjugation by increasing and/or decreasing the number of methine (-CH=) units between the two heterocycles.

h-Increasing and/or decreasing conjugation by increasing and/or decreasing the number of aza-methine (-CH=N-) units between the two heterocycles.

i-Changing the type of the heterocyclic quaternary salt residue employed in the reaction.

j-Changing the linkage position of the heterocyclic quaternary salt residue employed in the reaction.

k-Increasing and/or decreasing the number of the electronic charge transfer pathways inside the dyes molecules.

l-Increasing and/or decreasing the planarity of the dyes molecules.

m-Entering and/or introducing of either electron donating groups and/or electron withdrawing groups inside the dyes molecules.

n-Increasing and/or decreasing the number of the basic centers (electron pushing centers) inside the dyes molecules.

4. This review paper is recommended for chemists and researchers in the field of heterocyclic and/or cyanine dyes chemistry.

5. This paper review is recommended to all who are keen to have and know different methods in the synthesis of various classes of polyheterocyclic cyanine dyes and/or to get some basic applications, properties and characterization in the chemistry of cyanine dyes.

6. Because cyanine dyes have multi purposes uses and applications in various fields and different research area, this review paper is recommended not only for heterocyclic and/or cyanine dyes chemists but also for other scientists in other fields like biology, biotechnology, biochemistry, physics, engineering, pharmacology and medicine.

7. This review paper is recommended for all whom interested in the light absorbing systems in their research, labeling of biomolecules and/or in the synthesis and characterization of complex organic compounds.

8. This paper review is recommended to anyone interested in the subject, to chemistry libraries and also for the personal bookshelves of every organic heterocyclic and cyanine dyes chemist.

4. Current future development

The current and the future research developments aim to provide novel synthetic methods for the preparation of different classes of highly antimicrobial active, Anti-tumour, p-H sensitive, highly photographic sensitizers, non toxic, high stability, light fastness, near IR (Infrared), fluorescent, anti corrosion, strong labelled DNA and extra conjugated cyanine dyes. Such as oxadiazine cyanine dyes, thiazole cyanine dyes, metal stabilized cyanine dyes, pentamethine cyanine dyes, heptamethine cyanine dyes, nonamethine cyanine dyes, undecamethine cyanine dyes and tridecamethine cyanine dyes.

Also, the current and/or the future research developments aimed to provide new, novel and/or patent review papers in the field of color, dyes and pigments chemistry. The aimed review papers will covers and/or includes topics like the origin of color, the relation between color and constitutions, synthesis of dyes, properties of dyes, classification of dyes, uses and/or applications of dyes. Also, additional important topics for the current and/or the future research developments for the aimed review papers will includes methine cyanine dyes, hemi and/or styryl cyanine dyes, merocyanine dyes, apocyanine dyes, monoheterocyclic cyanine dyes, biheterocyclic cyanine dyes, polyheterocyclic cyanine dyes, six membered heterocyclic cyanine dyes, five/six membered heterocyclic cyanine dyes, five membered heterocyclic cyanine dyes and benz(naphth)/five membered heterocyclic cyanine dyes.

5. Conflict of interest

There is no conflict of interest.

6. Acknowledgements

I am thankful to the Chemistry department, Faculty of Science, Aswan University, Aswan, Egypt for supporting this work.

References

- Clark et al., 1997 – Clark S., Mathies R. (1997). *Anal Chem.*, 69: 1335.
- Abu El-Hamd, 1996 – Abu El-Hamd R.M. (1996). *Indian J. Heterocycl. Chem.*, 5(4), 297–304.
- Chen, 2006 – Chen R. (2006). The development and application of green dye, printing and dyeing, (6): 45.
- Deligeorgiev et al., 1995 – Deligeorgiev T.G., Gadjev N.I., Drexhage K-H., Sabnis R.W. (1995). *Dyes and Pigments*, 29: 315.
- Deligeorgiev et al., 1998 – Deligeorgiev T.G., Zaneva D.A., Kim S.H., Sabnis R.W. (1998). *Dyes and Pigments*, 37: 205-211.
- El-Aal et al., 2005 – El-Aal R.M., Koraiem A.I.M., Khalil Z.H., El-kody A.M.M. (2005). *Dyes and Pigments*, 66: 201-209.
- El-Maghraby et al., 1988 – El-Maghraby M.A., Khalafalla A.K., Hassan M.E., Soleiman H.A. (1988). *J. Chin. Chem. Soc. (Taipei)*, 35 (1): 53-56.
- El-Maghraby et al., 1991 – El-Maghraby M.A., Hassan M.E., Khalafalla A.K., Khalil M.A. (1991). *Asw. Sc. Tech. Bull.*, 12: 3-13.
- Gurrieri et al., 1997 – Gurrieri S., Wells S., Johnson, I., Bustamante C. (1997). *Anal Biochem.*, 249: 44.
- Hamer, 1964 – Hamer F.M. (1964). *The cyanine dyes and related components*, wiley, New York.
- Haugland, 1996 – Haugland R.P. (1996). *Handbook of fluorescent probes and research chemicals*. 6th ed Eugene, OR: Molecular Probes.
- Josef et al., 1996 – Josef M., Taylor J., McGown L., Pitner J.B., Linn C. P. (1996). *Biospectroscopy*, 2: 173.
- Khalafalla et al., 1993 – Khalafallah A.K., Koraiem A.I.M., El-Maghraby M.A. (1993). *Asw. Sci. Technol. Bull.*, 14, 3-18.
- Koraiem et al., 1999 – Koraiem A.I.M., Shindy H.A., Abu El-Hamd R.M. (1999). *Proc. Indian Academy of Sciences (Chem. Sci.)*, 111 (6): 709-724.
- Lee, 1997 – Lee L.G. (1997). (Biometric Imaging, Inc.). PCT Int Appl WO 97 17 471; *Chem Abstr.*, 127: 15178d.
- Lindsey et al., 1989 – Lindsey J. S., Brown P.A., Siesel D.A. (1989). *Tetrahedron*, 45 (15): 4845-4866.
- Millard et al., 1997 – Millard P., Roth B., Thi H-Ph T., Yue S., Haugland R.P. (1997). *Appl Environ Microbiol.*, 63: 2897.
- Mishra et al., 2000 – Mishra A., Behera R.K., Behera P.K., Mishra B.K., Behera G.B. (2000). Cyanines during the 1990s: A review. *Chem. Rev.*, 100: 1973.
- Moreda et al., 1997 – Moreda W., Forrester A.R. (1997). *Tetrahedron*, 57: 12595.
- Osman et al., 1997 – Osman A.M., Khalil Z.H., Koraiem A.I.M., Abu El-Hamd R.M., Abd El-Aal R.M. (1997). *Proc. Indian Acad. Sci. (Chem. Sci.)*, 109 (2): 115-134.
- Roth et al., 1997 – Roth B., Poot M., Yue S., Millard P. (1997). *Appl Environ Microbiol.*, 63: 2421.
- Roth et al., 1995 – Roth B., Millard P., Yue S., Wells S., Haugland R.P. (1995). (Molecular Probes, Inc.). PCT Int Appl WO 94 24 213. *Chem Abstr*, 122:163503t.
- Savarino et al., 1987 – Savarino P., Viscardi G., Barni E., Gaetano Di Modica G.D. (1987). *J. Heterocyclic Chem.*, 24: 1053-1060.
- Shindy et al., 2006 – Shindy H.A., El-Maghraby M.A., Eissa, F.M. (2006). *Dyes and Pigments*, 68 (1): 11-18.
- Shindy et al., 2014 – Shindy, H.A., El-Maghraby, M.A., Eissa, F.M. (2014). *Russ. Chem. Bull. [Izv. AN. Ser. Khim.]*, 63 (3), 707-715.

- Shindy et al., 2018 – Shindy H.A., El-Maghraby M.A., Goma M.M., Harb N.A. (2018). Synthesis, electronic transitions and antimicrobial activity evaluation of novel monomethine and trimethine cyanine dyes. *European Journal of Molecular Biotechnology*, 6 (2): 83-95.
- Shindy, 2007 – Shindy H.A. (2007). *Coloration Technology*, 123 (5): 298-305.
- Shindy, 2012 – Shindy H.A. (2012). Synthesis of different classes of five/five membered heterocyclic cyanine dyes: A Review paper. *Mini-Reviews in Organic Chemistry*, 9 (2): 209-222.
- Shindy, 2014 – Shindy H.A. (2014), Synthesis of different classes of six membered heterocyclic cyanine dyes: A Review. *Revue Roumaine de Chimie*, 59 (2): 117-123.
- Shindy, 2015 – Shindy H.A. (2015). Different Methods in the Synthesis of Mono(Bi)-Heterocyclic Six Membered Cyanine dyes: A Review. *Organic Chemistry. An Indian Journal*, 11 (1): 26-36.
- Shindy, 2015a – Shindy H.A. (2015). Synthesis of Different Classes of Benz (Naphth)/Five Membered Heterocyclic Cyanine Dyes: A Review. *Revue Roumaine de Chimie*, 60 (1): 5-13.
- Shindy, 2016 – Shindy H.A. (2016). Characterization, Mechanisms and Applications in the Chemistry of Cyanine Dyes: A Review. *European Journal of Molecular Biotechnology*, 14 (4), 158-170.
- Shindy, 2017 – Shindy H.A. (2017). Fundamentals in the Chemistry of Cyanine Dyes: A Review. *Dyes and Pigments*, 145: 505-513.
- Shindy, 2018 – Shindy H.A. (2018). Structure and solvent effects on the electronic transitions of some novel furo/pyrazole cyanine dyes. *Dyes and Pigments*, 149: 783-788.
- Shindy, 2018a – Shindy H.A. (2018). Novel polyheterocyclic cyanine dyes: synthesis, photosensitization and solvent/electronic transitions correlation. *European Reviews of Chemical Research*, 5 (1): 30-39.
- Timcheva et al., 1997 – Timcheva I.I., Maximova V.A., Deligeorgiev T.G., Gadjev N.I., Sabnis R.W., Ivanov I.G. (1997). *FEBS Letters*, 407: 141.
- Yarmoluk et al., 1996 – Yarmoluk I., Zhyvolup A., Koval'ska V., Klimenko I.I., Kukhareenko A., Koutun Yu., Slominsky Yu. (1996). *Biopolim kletka*, 12: 69.
- Yue et al., 1997 – Yue S., Singer V.I., Roth B., Mozer T., Millard P., Jones I.; Jin X., Haugland R.P., Poot, M. (1997). (Molecular Probes, Inc.). US Patent 5 658 751, 1997; *Chem Abstr.*, 127: 231608m.
- Yue et al., 1996 – Yue S., Singer V.I., Roth B., Mozer T., Millard P., Jones I., Jin X., Haugland R.P., Poot M. (1996). (Molecular Probes, Inc.). PCT Int Appl WO 96 13 552. *Chem Abstr.*, 125: 81256n.
- Yue et al., 1994 – Yue S., Johnson I., Huang Z., Haugaland R.P. (1994). (Molecular Probes, Inc.). US Patent 5 321 130. *Chem Abstr.*, 121:129393b.
- Zeng et al., 1997 – Zeng Zh., Clark S., Mathies R., Glazer A. (1997). *Anal Biochem.*, 252: 110.